Aalborg Universitet

AALBORG UNIVERSITY
DENMARK

A comparative evaluation of alternative optimization strategies for a novel heliostat-driven hydrogen production/injection system coupled with a vanadium chlorine cycle

Behzadi, Amirmohammad; Gholamian, Ehsan; Alirahmi, Seyed Mojtaba; Nourozi, Behrouz; Sadrizadeh, Sasan

Published in:
Energy Conversion and Management

DOI (link to publication from Publisher):
10.1016/j.enconman.2022.115878

Creative Commons License
CC BY 4.0

Publication date:
2022

Document Version
Publisher's PDF, also known as Version of record

Link to publication from Aalborg University

Citation for published version (APA):
Behzadi, A., Gholamian, E., Alirahmi, S. M., Nourozi, B., & Sadrizadeh, S. (2022). A comparative evaluation of alternative optimization strategies for a novel heliostat-driven hydrogen production/injection system coupled with a vanadium chlorine cycle. *Energy Conversion and Management*, *267*, Article 115878. https://doi.org/10.1016/j.enconman.2022.115878

General rights
Copyright and moral rights for the publications made accessible in the public portal are retained by the authors and/or other copyright owners and it is a condition of accessing publications that users recognise and abide by the legal requirements associated with these rights.

- Users may download and print one copy of any publication from the public portal for the purpose of private study or research.
- You may not further distribute the material or use it for any profit-making activity or commercial gain
- You may freely distribute the URL identifying the publication in the public portal -

Take down policy
If you believe that this document breaches copyright please contact us at vbn@aub.aau.dk providing details, and we will remove access to the work immediately and investigate your claim.

Energy Conversion and Management 267 (2022) 115878

Contents lists available at ScienceDirect

Energy Conversion and Management

journal homepage: www.elsevier.com/locate/enconman

A comparative evaluation of alternative optimization strategies for a novel heliostat-driven hydrogen production/injection system coupled with a vanadium chlorine cycle

Amirmohammad Behzadi [a,*], Ehsan Gholamian [b], Seyed Mojtaba Alirahmi [c], Behrouz Nourozi [a], Sasan Sadrizadeh [a,d]

[a] Department of Civil and Architectural Engineering, KTH University, Stockholm, Sweden
[b] Faculty of Mechanical Engineering, University of Tabriz, Tabriz, Iran
[c] Department of Chemistry and Bioscience, Aalborg University, Niels Bohrs Vej, Esbjerg 6700, Denmark
[d] School of Business, Society and Engineering, Mälardalen University, 72123 Västerås, Sweden

ARTICLE INFO

Keywords:
Concentrated solar power
Vanadium chlorine cycle
TEG
CO_2 emission reduction
Multi-objective optimization

ABSTRACT

This paper introduces an innovative and cost-effective multi-generation plant, driven by the central receiver-based concentrated solar systems, to facilitate the desired global green-transition process. The vanadium chlorine thermochemical cycle, which uses hydrogen instead of natural gas in the combustion chamber, is used as an innovative approach for reducing greenhouse gas emissions. The proposed system also includes a thermoelectric generator (TEG) for excess power generation and a multi-effect desalination (MED) unit to reduce exergy loss. The suggested system's technological, economic, and environmental metrics are analyzed and compared to a similar system that stores the created hydrogen rather than burning it in the combustion chamber. Furthermore, the viability of the studied model is investigated under the optimal operating condition, using the example of Sevilla in order to make the conclusions more reliable. According to the findings, the suggested novel configuration is a better alternative in terms of cost and environmental impact owing to decreased product energy costs and CO_2 emissions. The outcomes further indicate that the substitution of the condenser with TEG leads to considerably higher power production. According to the optimization findings, the multi-objective grey wolf algorithm is the best optimization strategy compared to the non-dominated genetic and particle swarm approaches. At the best optimization point, 2.5% higher exergy efficiency, 1 $/GJ cheaper product energy cost, and 0.12 kg/kWh lower levelized CO_2 emission are achieved compared to the operating condition. The Sankey diagram indicates that the solar heliostat system has the highest irreversibility. The exergy analysis results further reveal that the flue gas condensation process through the Rankine cycle and MED unit lead to a 53.2% reduction in exergy loss. Finally, considerable CO_2 emission reductions show that the suggested new method is an effective solution for cleaner energy production in warmer climate countries.

1. Introduction

The increase in fossil fuel use results in 120 ppm higher CO_2 concentration in the atmosphere and a global temperature rise of 2 °C until 2050 [1]. The deployment of renewable resources offers the most powerful and promising solution for achieving significant greenhouse gas emissions reduction [2]. According to the European environment agency (EEA), without renewable energy, since 2005, more than 10% higher emissions would have been obtained compared to the current value [3]. Based on the EEA roadmap 2050, European countries aim to supply more than 55% of total energy use from renewable resources, taking a major step toward decarbonization and green transition [4,43].

Solar energy, among other renewable resources, represents a clean and green energy source, with a growth rate of 33%. The central receiver-based concentrated solar (CRCS) systems are of great importance due to their high outlet temperature and cost-effectiveness [5]. They require a smaller area than other solar technologies for the same value of energy production [6]. Praveen [7] studied the feasibility of developing CRCS power systems for different regions in Saudi Arabia, concluding that the proposed 100 MW plant can entirely provide the power demand of the regions. In a recent study, Saghafifar et al. [8]

* Corresponding author.
E-mail address: abehzadi@kth.se (A. Behzadi).

https://doi.org/10.1016/j.enconman.2022.115878
Received 21 January 2022; Received in revised form 31 May 2022; Accepted 11 June 2022
Available online 18 June 2022
0196-8904/© 2022 The Author(s). Published by Elsevier Ltd. This is an open access article under the CC BY license (http://creativecommons.org/licenses/by/4.0/).

Nomenclature

A_h	Area of heliostat mirror (m^2)
A_r	Area of the solar receiver (m^2)
c	Exergy cost ($/GJ)
$\dot{C}$	Cost rate ($/hr)
C_P	Product energy cost ($/GJ)
D_P	Depletion factor
ΔT_{PP}	Pinch point temperature difference (K)
$\dot{E}$	Exergy rate (kW)
$ERTE$	Exergy round trip efficiency (%)
f	Exergoeconomic factor
h	Specific enthalpy (kJ/kg)
i_r	Interest rate
K	Thermal conductivity (W/(m.K))
$LCoE$	Levelized cost of electricity ($/(kWh))
n	Plant's operation years
N_{MED}	Number of MED effect
P	Pressure (kPa)
PR	Pressure ratio
$\dot{Q}$	Heat (kW)
SI	Sustainability index
TCR	Total cost rate ($/h)
T_b	Brine temperature (K)
U	Heat transfer coefficient (W/(m^2K))
V	Velocity (m/s)
$\dot{W}$	Power (kW)
Z	The investment cost of components ($)
$\dot{Z}$	Investment cost rate of component ($/hr)
ZT_M	Figure of merit

Subscript and abbreviations

AC	Air compressor
ANN	Artificial nueral network
BPE	Boiling point elevation
CC	Combustion chamber
Ch	Chemical
CI	Capital investment
Cond	Condenser
CRCS	Central receiver-based concentrated solar system
CRF	Capital recovery factor
D	Destruction
EES	Engineering equation solver
F	Fuel
GC	Gas cycle
GT	Gas turbine
IEA	International energy agency
MED	Multi-effect desalination unit
MOGWO	Multi-objective grey wolf optimizer
MOPSO	Multi-objective particle swarm optimizer
NEA	Non-equilibrium allowance
NSGA	Non-dominated sorting genetic algorithm
S	Sun
TEG	Thermoelectric generator
VCl	Vanadium coloride

Greek symbols

η_h	Heliostat optical efficiency
τ	Annual plant operation hours (hr)
ζ_{CO2}	Levelized CO_2 emission (ton/MWh)

examined the techno-economic-environmental assessment of a dual-receiver solar power plant equipped with a heliostat field. They reported a lower CO_2 emission index and reduced energy cost compared to the same solar technologies. Considering the case of Los Angeles, an innovative combined power and hydrogen generation system driven by the CRCS system was introduced by Alirahmi et al. [6], showing that the proposed solar system prevents the annual CO_2 emission of 3313 tons at the acceptable payback period of 4.6 years.

The main pollutant problem associated with fuel combustion is the formation of nitrogen oxides (NOx) during combustion. NOx is involved in the development of acid rain as well as local air pollution. Using hydrogen is one technique to lower NOx emissions [9,10]. Thermochemical water-splitting cycles are more efficient, cost-effective, and environmentally acceptable than other new hydrogen-generation technologies. Several researchers have studied the techno-economic assessment of different solar-assisted thermochemical cycles for hydrogen production. Oruc and Dincer [11] recently studied a solar-driven Sodium hydroxide (NaOH) thermochemical cycle from the quantity/quality of energy conversion facets. They achieved energy and exergy efficiencies of 80% and 82% for the proposed hydrogen production cycle, respectively, which is considerable. In another study, Sadeghi et al. [12] proposed and optimized a thermochemical hydrogen cycle equipped with a heliostat solar field and thermal energy storage units. They revealed that combining the CRCS system with the Copper(I) chloride (CuCl) cycle is potentially an excellent solution for efficient hydrogen generation. Balta et al. [13] investigated and compared the thermodynamic metrics of different chlorine cycles, including CuCl, FeCl, VCl, and MgCl. They demonstrated that hydrogen production via the vanadium–chlorine (V–Cl) cycle is the best and most promising approach due to it having the highest efficiency of 40%.

Integrating thermoelectric generators (TEG) with a conventional power system and solar-driven cycles is a promising method of improving efficiency and mitigating environmental pollution and energy cost by directly generating valuable electricity from waste heat [14]. Habibollahzade et al. [15] studied the impact of using a TEG unit instead of the condenser of a solar-based thermochemical hydrogen system and concluded that a lower levelized energy cost and higher performance efficiencies are achieved compared to the same system without TEG. Demir and Dincer [16] analyzed a hybrid solar system comprising CRCS equipped with a heliostat field, TEG unit, and proton exchange membrane (PEM) electrolyzer and showed that TEG provides around 7% of the total power generation. Khanmohammadi et al. [17] conducted a comparative sensitive analysis of an innovative solar-based cogeneration system and highlighted the impact of recovering low-temperature waste heat via TEG. They revealed higher produced power and energy efficiency of 3.27 kW and 6.8%, respectively, are obtained by adding TEG units. Behzadi et al. [18] examined the techno-economic assessment of an innovative solar-based system integrated with the TEG unit. They reported that a lower payback period of 2.4 years and higher hydrogen generation of 0.023 kg/Day is achieved if the TEG unit replaces the condenser.

Another significant consequence of climate change and global temperature increment is the lack of adequate access to potable water as a first-order necessity that highly affects human life. According to Fakhari et al. [19], 3% of the water on the earth is potable water, of which only half is reachable. For this, in addition to electricity production from a renewable resource, more attention should be paid to the cogeneration of potable water through different desalination processes for bringing down the effect of climate change, growing population, and drought. In comparison to electricity-driven processes, thermal-based desalination technologies are a promising and popular option due to the importance of the waste heat recovery process as an energy enhancement and cost reduction approach. Youssef et al. [20] conducted a techno-economic-environmental comparison of various desalination processes and

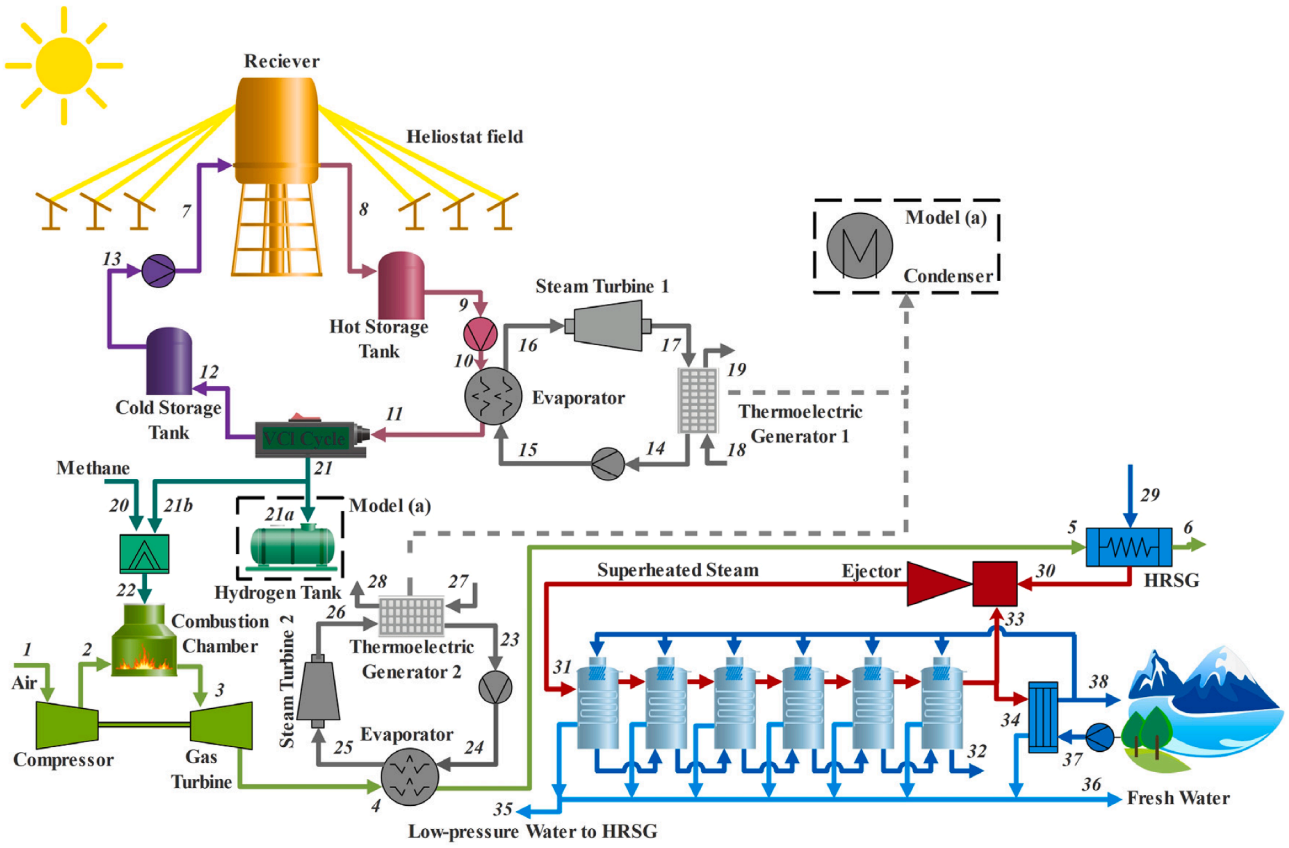

Fig. 1. Schematic representation of the studied models.

concluded that heat-driven technologies are superior due to lower environmental impact and better water quality. The multi-effect desalination (MED) unit is techno-economically superior to other thermal-driven desalination machines, offering lower investment costs and energy use. Chitgar and Emadi [21] recently proposed an innovative multi-generation system and concluded that a MED unit with an hourly production of 5.6 m^3 is the most appropriate option for potable water generation from low-temperature exhaust gases. Having assessed and compared the influence of adding a MED unit for exploiting the waste heat of a low-temperature heat source, Aguilar-Jimenez et al. [22] attained a higher performance efficiency of 22% compared to the single-generation power cycle.

Despite the intensive interest and extensive works investigating multi-generation solar-based systems applying different technologies, the existing literature still struggles with a few critical issues. First, performance improvement and heat loss reduction of solar systems should be prioritized to reduce trade barriers and promote high-quality solar thermal products. Second, the power productivity of renewable-driven systems on top of every other output needs to be improved. Third, practical and promising active/passive efficiency improvement methods, like exploiting the low-temperature waste heat, must be applied to mitigate the energy costs to increase the motivation for using solar-driven technologies. The last important issue is making the existing hybrid systems more environmentally friendly to take a major step towards the green transition. To address these issues, the present work introduces an innovative, efficient, and environmentally friendly renewable-based system for multi-generation of power, hydrogen, and potable water. The central receiver-based concentrated solar systems drive the proposed system with high outlet temperature, low heat production, and investment costs. Also, a new greenhouse gas emission reduction method is implemented through the vanadium chlorine thermochemical cycle, using hydrogen instead of natural gas in the combustion chamber. Moreover, the studied system is equipped with a thermoelectric generator and multi-effect desalination unit, respectively, for active and passive production of surplus power and potable water from low-temperature waste heat. The performance of the proposed model is studied and compared against the condenser-based system that stores the produced hydrogen instead of consuming it in the combustion chamber. For this, a comparative parametric study is performed to determine the superior model and evaluate the influence of main operational parameters on techno-economic-environmental aspects. Afterward, multi-objective optimization based on NSGA-II, MOPSO, and MOGWO algorithms is applied to the superior model to compare the performance of each optimization approach and determine the best operating condition. Eventually, to make the results more reliable, the feasibility of the best model is studied under the optimum design parameters considering the real-time weather data information of Sevilla.

2. Proposed studied systems

Fig. 1 shows a schematic diagram of the proposed innovative hybrid system (Model (b)). As depicted, the studied system comprises the central receiver-based concentrated solar system for heat production; the vanadium chlorine thermochemical cycle for hydrogen generation; the gas turbine and Rankine cycles and thermoelectric generators for power production; and the multi-effect desalination unit for potable water generation from low-temperature waste heat. In the CRCS system, the solar radiation is concentrated by the heliostat field into the receiver mounted on the top of the tower, which absorbs and transfers the heat to the hot storage tank. The heliostat field consists of flat movable mirrors equipped with dual-axis sun-tracking systems, leading to higher outlet temperature due to the higher concentration ratio than other solar technologies. The produced heat is first used in the evaporator to run the

Table 1
Input values of design parameters [41,42].

Parameter	Value	Parameter	Value
CRCS		**Rankine**	
N_{HEL}	350	P_{16} (kPa)	3500
A_h (m^2)	121	T_{17} (K)	373.15
A_r (m^2)	60	$\Delta T_{PP,Cond}$ (K)	5
η_h (%)	71	$\eta_{is,Pump}$ (%)	80
ε (%)	80	$\eta_{is,ST}$ (%)	85
$T_{Receiver}$ (K)	1323.15	**Gas cycle**	
MED		$\dot{W}_{net,GC}$ (kPa)	2000
N_{MED} (-)	7	PR (-)	6
T_{b1} (K)	334.95	T_{CC} (K)	1473.15
T_{35} (K)	313.15	$\eta_{is,AC}$ (%)	87
T_{36} (K)	303.15	$\eta_{is,GT}$ (%)	89
T_{bN} (K)	315.95	**VCl cycle**	
TEG		$T_{step\ 1}$ (K)	798
$\Delta T_{PP,TEG}$ (K)	5	$T_{step\ 2}$ (K)	373
ZT_M	0.85	$T_{step\ 3}$ (K)	573

Rankine cycle and then transmitted to the VCl unit to start the thermochemical cycle for hydrogen production. The generated hydrogen is consumed as the combustion chamber's secondary fuel, which is primarily driven by natural gas. Using this method (Model (b)) – that is, replacing traditional natural gas with hydrogen – a considerable reduction of carbon dioxide emission is attained, making the proposed system green and environmentally promising. In the gas-based power system, after being compressed (State 2), the inlet air goes into the combustion chamber to be mixed with hydrogen (State 21b) or natural gas (State 20). The combustion products with a high enthalpy value then enter the turbine to generate the power. The turbine outlet exhaust gases move into the evaporator to run a steam Rankine cycle. In the studied Rankine cycles, the condensers are replaced by the TEG units to harvest waste heat for extra power production. The evaporator outlet gases are still valuable to run a MED system through a flue gas condensation process in the heat recovery steam generator (HRSG) unit. As indicated in Fig. 1, the heat-driven MED system consists of a steam ejector, flash boxes, and condenser.

In the ejector, the primary steam with high enthalpy (State 30) is mixed with the secondary vapor (State 33) coming from the last stage. The generated superheated steam (State 31) with a mean pressure is used as the heat source of the first stage. On the other hand, the inlet seawater (State 37) enters the condenser for liquefaction of desalinated vapor (State 34) from the last step. Subsequently, while an equal portion of the preheated seawater is divided between the stages as the feedwater, the remaining stream returns to the sea (State 38). The heat is transferred from the superheated steam (State 31) to the feedwater to obtain the boiling point in the first stage. The generated steam goes into the second stage as the heat source for the evaporation process. The remaining brine then moves into the next stage to improve system performance and generate more vapor. A small amount of condensed vapor is again evaporated at a lower pressure to be mixed with the generated vapor. This process is repeated in the subsequent stages to produce the ultimate potable water. According to Fig. 1, the same system (Model (a)) equipped with the condenser and hydrogen tank is also proposed to investigate and compare the impact of adding a TEG unit (instead of a condenser) and consuming hydrogen (instead of storing it).

Before performing the techno-economic-environmental calculations, the following assumptions were made to accomplish the thermodynamic modeling of each model:

- Each component's reaction temperature and pressure equal 298 K and 100 kPa, respectively.
- The variation of potential and kinetic energy is overlooked.
- The heat input for step 1 in the VCl cycle shall be 130% of the heat required to split $2VCL_3$ into $2VCL_2$ and CL_2 [13,23].
- Heat loss in the heat exchangers and pressure mitigation within the pipes are neglected.
- In each effect, the vapor produced is fully desalinated.
- All of the effects have the same temperature difference.
- The salinity of seawater and the maximum salinity of brine are 36% and 70%, respectively.

The values of input parameters for each subsystem, including the CRCS system, VCl and Rankine cycles, and TEG and MED units, are tabulated in Table 1.

3. Methodology

Engineering equation software (EES) was implemented to calculate techno-economic-environmental equations of the studied innovative system. Using the MATLAB program (version R2021b), multi-objective optimization based on different approaches was then performed to maximize exergy efficiency while simultaneously minimizing the product energy cost and levelized CO_2 emission index.

3.1. Energy assessment

Performance evaluation was carried out by writing the energy and mass balances contemplating each component as a lumped control volume, as follows [24]:

$$\sum \dot{m}_{in} = \sum \dot{m}_{out} \tag{1}$$

$$\dot{Q} - \dot{W} = \sum \dot{m}_{out} h_{out} - \sum \dot{m}_{in} h_{in} \tag{2}$$

In this equation, $\dot{m}$ is the mass flow rate entering/leaving each component and $\dot{W}$ and $\dot{Q}$ are the rate of produced/received power and heat, respectively.

3.1.1. Solar heliostat system

Due to a very high concentration ratio, the CRCS system consisting of a heliostat field and solar receiver is a very efficient, cost-effective, and wise solution to produce a considerable amount of heat per area and increase the contribution of solar energy practice. Defining N_{HEL} as the number of mirrors in the solar field, the received solar energy by the heliostat field is calculated as follows [25]:

$$\dot{Q}_h = \eta_h \times A_h \times N_{HEL} \times I \tag{3}$$

where η_h, A_h, and I are the efficiency, total area of the mirrors, and incident solar radiation, respectively. Since a portion of the received heat is wasted in the environment, the heat absorbed by the receiver is not equal to the heat delivered by the heliostat field. Therefore, the heat lost to the ambient is evaluated using Eq. (4) [25]:

$$\dot{Q}_{Loss} = h_{air} A_r (T_{Recievер} - T_0) + \sigma A_r \varepsilon (T^4_{Recievер} - T^4_0) \tag{4}$$

In this equation, A_r is the collector's surface area and $T_{Reciever}$ denotes the surface temperature. Moreover, h_{air} indicates the convective heat transfer of the air, which is a function of wind velocity, as follows [6]:

$$h_{air} = 10.45 - V_{air} + 10\sqrt{V_{air}} \tag{5}$$

Finally, the heat received by the working fluid can be assessed by [6]:

$$\dot{Q}_r = \dot{Q}_h - \dot{Q}_{Loss} = \dot{m}(h_8 - h_7) \tag{6}$$

3.1.2. Vanadium chlorine thermochemical cycle

The VCl cycle is a heat-driven thermochemical system first studied by McRea and his research group for hydrogen generation at the highest operating temperature. This cycle mainly comprises three reactions at different temperature levels (low-, moderate, and high-temperature)

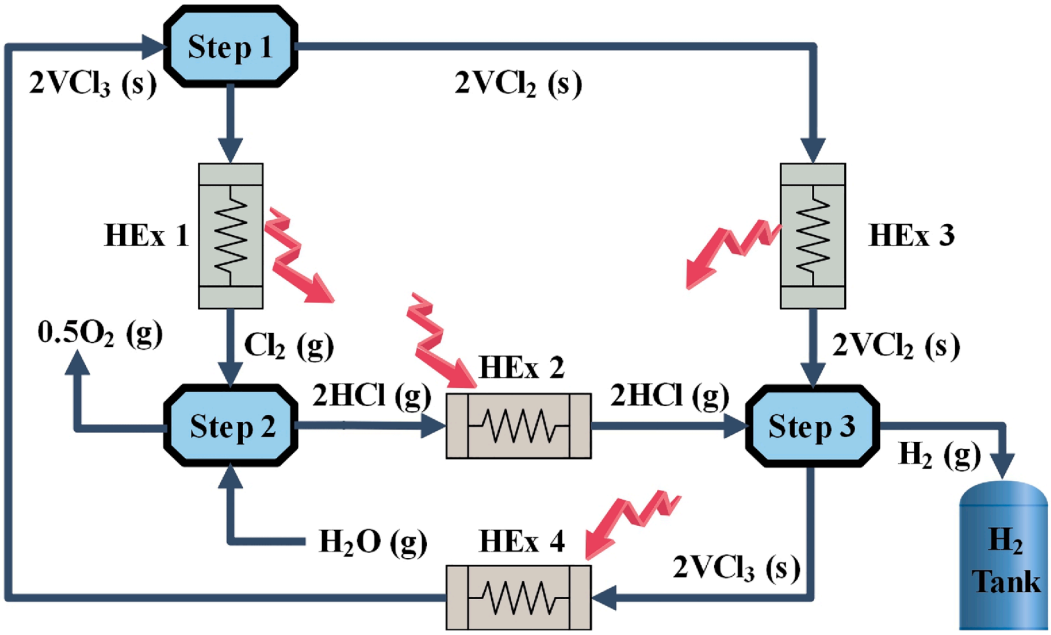

Fig. 2. Schematic layout of VCl cycle.

that occur in three steps, as illustrated in Fig. 2. According to the figure, in the first step, vanadium (III) chloride (solid) is decomposed to vanadium(II) chlorine (solid) and chlorine gas at the maximum temperature of 798 K as follows [26]:

$$2VCl_3(s) \rightarrow 2VCl_2(s) + Cl_2(g) \tag{7}$$

Fig. 2 further indicates that, in the second step, the produced chlorine gas at the previous step reacts with steam to generate hydrogen chloride and oxygen gases at the low temperature of 373 K, as written by [26]:

$$Cl_2(g) + H_2O(g) \rightarrow 2HCl(g) + 0.5O_2(g) \tag{8}$$

Finally, at the moderate temperature of 573 K, hydrogen (the desired component) and vanadium (III) chloride are produced from the reactions of hydrogen chlorine gas and vanadium(II) chlorine in the solid-state, as follows [26]:

$$2VCl_2(s) + 2HCl(g) \rightarrow 2VCl_3(s) + H_2(g) \tag{9}$$

The sum of the above steps is the main reaction in the thermochemical cycles, called the water-splitting reaction, on which the steam is decomposed into oxygen and hydrogen, as expressed in Eq. 10:

$$H_2O(g) \rightarrow 0.5O_2(g) + H_2(g) \tag{10}$$

3.1.3. Thermoelectric generator

TEG is an advanced technology used in thermal energy systems to directly convert waste heat into surplus electricity via the Seebeck effect. It is a reliable energy source with a silent operation, enhancing the system efficiency and environmental friendliness while reducing the production cost. Defining the figure of merit (ZT_M) as a quantitative parameter to examine a device's performance compared to its alternative, the TEG efficiency is calculated by Eq. (11) [27]:

$$\eta_{TEG} = \eta_{Carnot}\frac{\sqrt{1+ZT_M}-1}{\sqrt{1+ZT_M}+\frac{T_c}{T_h}} \tag{11}$$

$$ZT_M = \frac{\psi^2 T_m}{K_t R} \tag{12}$$

$$T_M = \frac{1}{2}(T_c + T_h) \tag{13}$$

$$\psi = \frac{-\Delta V}{\Delta T} \tag{14}$$

$$\eta_{Carnot} = 1 - \frac{T_c}{T_h} \tag{15}$$

where T_c and T_h are the cold and hot side temperatures, respectively. Also, K_t and R denote the thermal conductivity and the thermal resistance inside the TEG. Eventually, TEG output power as a function of efficiency and the transferred heat is evaluated as follows [27]:

$$\dot{W}_{TEG} = \eta_{TEG}\dot{Q}_{TEG} \tag{16}$$

3.1.4. Multi-effect desalination unit

The MED system is a promising and cost-effective choice for potable water production because it has reduced energy use and lower temperature than similar technologies. To accomplish the MED unit modeling, a set of balance equations, including mass, salinity, and energy, were solved for each subsystem. The temperature difference across different effects can be computed by defining T_{b_1} and T_{b_N} as the brine temperature at the 1st and N^{th} effects [28]:

$$\Delta T = \frac{T_{b_1} - T_{b_N}}{N-1} \tag{1}$$

Furthermore, the brine and the water vapor temperatures at the subsequent effect are assessed by [28]:

$$T_{b_{i+1}} = T_{b_i} - \Delta T \tag{2}$$

$$T_{vi} = T_{bi} - BPE \tag{3}$$

here, BPE denotes the boiling point elevation. The cooldown temperature of brine ($T_i^{'}$), which is the sum of the non-equilibrium allowance (NEA_i) and the brine temperature (T_{b_i}), is expressed by [28]:

$$T_i^{'} = T_{b_i} + NEA_i \tag{20}$$

For the steam ejector, the energy balances can be written as [29]:

Table 2
Mass and energy balance equations for each effect of the MED unit [28,29].

1st effect	Mass balance	$B_1 = F_1 - D_1$
	Salinity balance	$X_1 = \frac{F_1}{B_1}X_f$
	Energy balance	$M_m L_m = D_1 L_1 + F_1 C_P (T_1 - T_F)$
2 to N effect	Mass balance	$B_i = B_{i-1} + F_i - D_i$
	Salinity balance	$X_i = \frac{F_i}{B_i}X_f + \frac{B_{i-1}}{B_i}X_{i-1}$
	Energy balance	$(D_{i-1} + D'_{i-1})L_{i-1} = D_i L_i + F_i C_P (T_i - T_F) + B_i C_P (T_i - T_{i-1})$

$$M_m h_m + D_r h_g = (M_m + D_r) h_s \tag{21}$$

The thermodynamic equations for each effect of the MED unit, as well as the condenser, are tabulated in Table 2.

For the 1st and 2nd to Nth effect and the condenser, the formula of areas of heat transfer that were prerequisites to accomplishing the MED modeling is expressed by [29]:

$$A_1 = \frac{M_s L_s}{U_{e1}(T_S - T_1)} \tag{4}$$

$$A_i = \frac{(D_{i-1} + D'_{i-1})L_{i-1}}{U_{ei}\Delta T_i} \tag{5}$$

$$A_C = \frac{(D_N + D'_N - D_r)L_W}{U_c LMTD_C} \tag{6}$$

here U_e denotes the overall heat transfer coefficient of the ith effect, and U_c is the heat transfer coefficient of the condenser and can be calculated as follows [29]:

$$U_e = 1.9394 + 1.40562 \times 10^{-3} \times T_b - 2.07525 \times 10^{-5} \times T_b^2 + 2.3186 \times 10^{-6} \times T_b^3 \tag{7}$$

$$U_c = 1.7194 + 3.2063 \times 10^{-3} \times T_V + 1.5971 \times 10^{-5} \times T_V^2 + 1.9918 \times 10^{-7} \times T_V^3 \tag{8}$$

3.2. Exergy-sustainability assessment

Exergy evaluation based on the second law of thermodynamics was applied to examine the merit of energy conversion and deviation of the studied system from ideal performance. For this, the rate of irreversibility, exergy efficiency, and sustainability index was calculated. Defining e, $\dot{E}_Q$, $\dot{E}_W$, and $\dot{E}_D$ as the inlet/outlet stream exergy, the exergy of heat, the exergy of work, and exergy destruction, respectively, the balanced equation is written as below [30]:

$$\dot{E}_Q - \dot{E}_W = \sum \dot{m}_{out} e_{out} - \sum \dot{m}_{in} e_{in} + \dot{E}_D \tag{27}$$

It was assumed that the potential and kinetic energies are overlooked due to the system's rests relative to the environment. So, the stream exergy equals the sum physical (e^{ph}) and chemical (e^{ch}) exergy, as calculated by Eq. (29) and Eq. (30) [31]:

$$e = e^{ph} + e^{ch} \tag{28}$$

$$e_i^{ph} = (h_i - h_0) - T_0(s_i - s_0) \tag{29}$$

$$e_i^{ch} = \sum_{i=1}^{n} x_i e_{0.i}^{ch} + RT_0 \sum_{i=1}^{n} x_i \ln(x_i) \tag{30}$$

here, $e_{0.i}^{ch}$ is the standard chemical exergy (see Appendix B), and x_i is the mole fraction of the gaseous stream. According to Eq. (31), the ratio of exergy of product to the exergy of fuel is defined as the exergy efficiency (ε_i), another vital parameter for irreversibility analysis of each component [31].

$$\varepsilon_i = \frac{\dot{E}_{P,i}}{\dot{E}_{F,i}} \tag{31}$$

After applying a complete exergy evaluation to each component, the sustainability index was calculated to determine the influence of irreversibility reduction on the improvement of the overall system's environmental friendliness, as below:

$$SI = \frac{1}{D_P} \tag{32}$$

$$D_P = \frac{\sum_{k=1}^{n_k} \dot{E}_{D,k}}{\dot{E}_{in}} \tag{33}$$

In this equation, D_p denotes the depletion factor, which is the ratio of the overall system's exergy destruction to the input exergy rate. Also, $\dot{E}_{in}$ is the sum of the exergy of the sun received by the heliostat field and the exergy of input fuel, as follows:

$$\dot{E}_{in} = \dot{E}_S + \dot{E}_F \tag{34}$$

$$\dot{E}_S = \left[1 + \frac{1}{3}\left(\frac{T_0}{T_S}\right)^4 - \frac{4}{3}\left(\frac{T_0}{T_S}\right)\right]\dot{Q}_r \tag{35}$$

$$\dot{E}_F = \dot{m}_{Methane} e_{Methane}^{ch} \tag{36}$$

here, T_S is the temperature of the sun, which is equal to 5770 K. Finally, the overall exergy efficiency is calculated as the ratio of the net produced exergy to the input exergy:

$$\eta_{II,Overall} = \frac{\dot{E}_{out}}{\dot{E}_{in}} \tag{37}$$

$$\dot{E}_{out} = \dot{W}_{ST,1} + \dot{W}_{GT} + \dot{W}_{ST,2} + \dot{W}_{TEG,1} + \dot{W}_{TEG,2} + \dot{E}_{35} - \sum \dot{W}_{Pm} - \dot{W}_{comp} \tag{38}$$

Because different components of the proposed system operate at two different periods, exergy round trip efficiency (ERTE) is defined to evaluate the system comprehensively as follows:

$$ERTE = \frac{\dot{E}_{out} \times 24[hr]}{\dot{E}_F \times 24[hr] + \dot{E}_S \times 10[hr]} \tag{39}$$

3.3. Economic-environmental assessment

After applying thermodynamic equations and finding the performance indicators, an economic evaluation of the studied system was conducted using the specific cost theory. Accordingly, the cost of each component is divided into the operating and maintenance (OM), and capital investment (CI) costs as follows [32]:

$$\dot{Z}_k = \dot{Z}_k^{OM} + \dot{Z}_k^{CI} \tag{40}$$

Defining γ and τ as the fixed OM costs coefficient and the system's operating hours in the whole year, respectively, $\dot{Z}_k^{OM}$ is calculated by the following equation [32]:

$$\dot{Z}_k^{OM} = \left(\frac{\gamma_k}{\tau}\right) Z_k \tag{41}$$

Also, the capital investment costs ($\dot{Z}_k^{CI}$) is defined as written below [33]:

$$\dot{Z}_k^{CI} = \left(\frac{CRF}{\tau}\right) Z_k \tag{42}$$

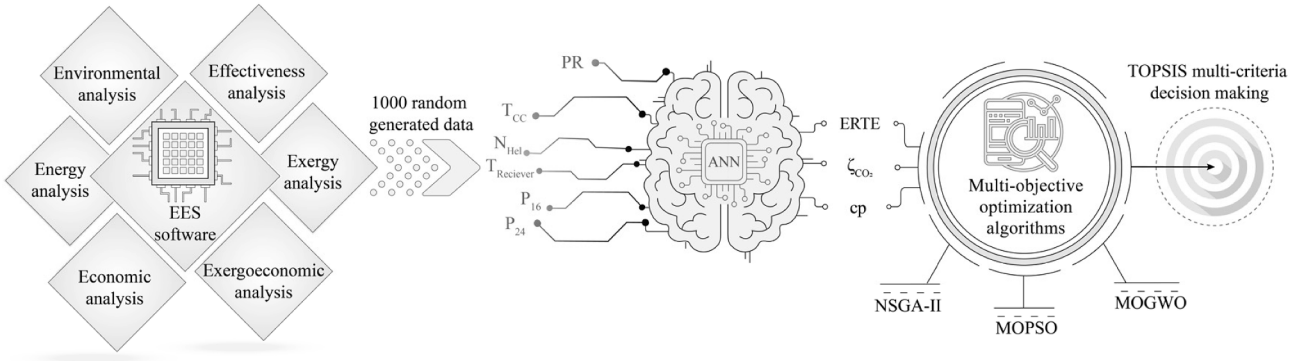

Fig. 3. Flowchart diagram of the optimization procedure.

Table 3
The range of significant decision parameters for optimization.

Variable	Description	Lower bound	Higher bound
***PR* (-)**	Pressure ratio	6	12
T_{CC} **(K)**	Combustion temperature	1200	1500
N_{Hel} **(-)**	Number of heliostat	300	400
$T_{Reciever}$ **(K)**	Receiver temperature	1100	1300
P_{16} **(kPa)**	Turbine 1 inlet pressure	2500	4000
P_{24} **(kPa)**	Turbine 2 inlet pressure	2500	4000

$$CRF = \frac{i(1+i)^n}{(1+i)^n - 1} \tag{43}$$

In this equation, CRF denotes the capital recovery factor calculated based on the interest rate (i) and the system's operation years (n). The cost of each component at the present year was calculated using Marshal and Swift's formula based on the cost indexes at the reference year (CI^{RY}) and the present year (CI^{PY}), as follows [34]:

$$\dot{Z}_k^{PY} = \left(\frac{CI_{PY}}{CI_{RY}}\right) \dot{Z}_k \tag{44}$$

Z_k is the purchased cost in the above equations, which is evaluated as listed in Table A1 (see Appendix A). Moreover, the total cost rate (*TCR*) as an important economic metric, which is the sum of components' cost ($\dot{Z}$) and the fuel cost ($\dot{C}_F$), is calculated as below:

$$TCR = \sum_{k=1}^{n_k} \dot{Z}_k + \sum_{i=1}^{n_F} \dot{C}_{F_i} \tag{45}$$

Finally, the cost-effectiveness of the studied innovative hybrid system was examined, calculating the product energy cost in $/GJ and levelized cost of electricity as follows:

$$C_P = \frac{TCR}{\dot{E}_{out}} \tag{46}$$

$$LCoE = \frac{TCR}{\dot{W}_{ST,1} + \dot{W}_{GT} + \dot{W}_{ST,2} + \dot{W}_{TEG,1} + \dot{W}_{TEG,2}} \tag{47}$$

As mentioned, the main novelty of this work was the introduction of a clean multi-generation system by adding a solar system and substitution of hydrogen with methane fuel. For this, the levelized carbon dioxide emission (ζ_{CO2}) in tons per MWh was assessed to investigate and compare the environmental friendliness of the proposed innovative system with the conventional methane-driven plant:

$$\zeta_{CO_2} = \frac{\dot{m}_{CO_2}}{\dot{E}_{out}} \tag{48}$$

here, $\dot{m}_{CO_2}$ is the generated carbon dioxide emitted into the atmosphere.

3.4. Optimization model

The optimization goal is to ascertain the most favorable operating condition relative to a set of constraints or significant criteria. These contain maximizing functions like net generated energy, performance efficiencies, and sustainability index while minimizing unfavorable objectives such as carbon dioxide emission and energy costs. While single-objective optimization (SOO) aims to find the best condition satisfying a unique indicator standalone, multi-objective optimization (MOO) extends the optimization theory by considering individual objectives simultaneously. Fig. 3 demonstrates the optimization methodology applied to the present work. According to the figure, the mathematical model of techno-economic-environmental equations was carried out in EES software with an extensive library of thermodynamics properties of various fluids. However, because EES cannot solve MOO problems, the MATLAB program was linked to accomplishing the optimization algorithm. Because the integration of EES with MATLAB requires a long run time to conduct the optimization, an artificial neural network (ANN) approach was added to solve the problem at the minimum time, as shown in Fig. 3. As a robust computational method, ANN is applied to various applications, including the optimization of energy systems, because of the capability to solve nonlinear problems with maximum accuracy and minimum cost. ANN works based on a controlling procedure that tries to find the most successful connections between the layers (input, hidden, and output) with the minimum failure by repeating the process. After applying thermodynamic, exergoeconomic, and environmental evaluations in EES, 1000 random data points, including the input (the main design parameters) and output (significant objective functions), were introduced to the ANN. Then, an ANN model based on six hidden layers was implemented to fit the inputs and forecast the outputs. Subsequently, the training process was carried out to extract the mathematical correlation between the design parameters and expected outputs. Eventually, the extracted training network was given to the MOO algorithm as a fitness function to start the optimization.

The best operating condition from techno-economic-environmental viewpoints was ascertained using three optimization algorithms: NSGA-II, MOPSO, and MOGWO. This not only determined the optimum system sizing but also investigated and compared the performance of each algorithm. Among different MOO approaches, NSGA-II, based on a conventional genetic algorithm, has been widely used and investigated by many decision-makers due to the high calculation and fitness rates and the ability to solve challenging problems. Flexibility is the main feature of NSGA-II because it finds the solution without any comprehensive understanding of the problem's structure and variables. MOPSO is a stochastic optimization approach based on a swarm with better diversity and faster convergence that has been extensively applied to engineering problems. Population, exploration, turbulence factor, and polynomial mutation are the basic concepts of this approach. The main competency of this powerful technique is its ability to accurately solve

Table 4
Comparative validation of VCl cycle.

Step number	Step temperature (K)	Reaction heat demand (kJ/mole H_2)		
		Balta et al. [13]	Present study	Error (%)
1	798	349.6	350.02	0.12
2	373	70.77	71.1	0.46
3	573	−88.72	−88.05	0.75

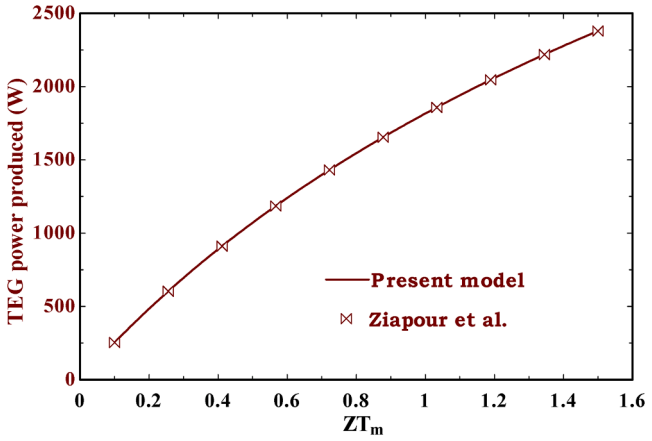

Fig. 4. Comparison of the performance indicators of the present TEG unit against the results reported by Ziapour et al. [35].

Table 5
Comparison of the present MED model with a real plant.

Design conditions	Present model	Real plant [36]
Effect numbers	6	6
Motive steam rate (kgs^{-1})	21.20	21.20
The pressure of motive steam (bar)	25	25
Minimum temperature of brine (°C)	42.8	42.8
Top brine temperature (°C)	61.80	61.80
Seawater temperature (°C)	30	30
Performance indicators		
Desalinated water (kg/s)	188.2 4	184.4
Gain output ratio	8.78	8.6

complicated nonlinear problems. The final optimization tool is MOGWO, a new potent approach inspired by the hunting behavior of grey wolves. MOGWO outperforms the existing multi-objective methods in the aspect of technical and economic benefits like robustness, convergence, lower computational costs, and spacing. Table 3 indicates the logical range of significant design parameters and desired performance metrics for optimization purposes. As listed, at the best optimization point, the exergy round trip efficiency should be maximized, and the product energy cost and levelized CO_2 emission must be minimized simultaneously.

4. Results and discussion

A comparative parametric study was conducted to better indicate the influence of hydrogen injection on techno-economic-environmental metrics with the variation of main operating parameters. For this, the impacts of compressor pressure ratio (r_P), combustion temperature (T_{CC}), receiver temperature ($T_{Reciever}$), turbine inlet pressure, and the number of MED effects (N_{MED}) on the exergy round trip efficiency (*ERTE*), product energy cost (C_P), a net produced power ($\dot{W}_{net}$), the levelized carbon dioxide emission (ζ), the generated potable water, and sustainability index (*SI*) were investigated in detail. NSGA-II, MOPSO, and MOGWO algorithms were then applied to optimize the superior model and examine and compare the performance of each optimization approach. The Sankey diagram depicts the exergy flow throughout the system and each component's destruction/loss rate under the best operating condition (TOPSIS point). Eventually, the feasibility of the superior model is studied under the real weather data information of Sevilla.

4.1. Validation

In Table 4, the comparison of the reaction heat demands in each step under the same operating condition is investigated against Balta et al. [13] results to validate the VCl thermochemical cycle. According to the table, a good agreement between the results is achieved since the error percentage is less than 1. The validation of TEG is depicted in Fig. 4, in which the variation of TEG power produced with the figure of merit is studied and compared. The figure shows that the present model results are analogous to the results attained by Ziapour et al. [35]. Finally, the performance of the MED unit is validated against the data of a real plant, as tabulated in Table 5. It can be observed that almost the same results are achieved for the same values of design parameters, indicating the present model's precision.

4.2. Comparative parametric study

The effect of the gas cycle pressure ratio on each model's performance metrics is depicted in Fig. 5. Increasing the pressure ratio increases the enthalpy of combustion products. Therefore, based on the first law of thermodynamics, the mass flow rate decreases at constant power. Thereafter, when a lower mass flow rate enters the evaporator and HRSG, the heat transferred to the Rankine cycle and MED unit decreases; hence, a net power produced and potable water will decrease, as illustrated in Fig. 5. According to Fig. 5, for both models, a higher round trip exergy efficiency of 5% is attained by increasing the gas cycle pressure ratio from 4 to 15. This is reasonable given that the lower mass flow rate of combustion products requires lower inlet methane. So, the exergy efficiency and the sustainability index will increase based on Eq. (39) and Eq. (32), respectively. Moreover, Fig. 5(b) presents that a favorable environmental condition is achieved when the pressure ratio rises because the mitigation of CO_2 emission is lower than the reduction of power produced (look at Eq. (48). The figure further shows that as the pressure ratio increases, the product energy cost increases due to the decrement of power production. According to Fig. 5, in the whole domain of pressure ratio, the proposed innovative system (Model (b)) is superior to the conventional system in economic and environmental terms due to the lower product energy cost and levelized carbon dioxide emission. Moreover, Fig. 5 indicates the importance of adding the thermoelectric generator for direct waste heat deployment due to the proposed system's higher power production than the condenser-based model. However, a higher ERTE and potable water generation are obtained if the hydrogen does not charge the bottom cycle.

Since the performance of the combustion chamber is highly affected by the thermodynamic properties of the outlet products, the effect of combustion temperature on each model is shown and compared in Fig. 6. As the figure shows, when the combustion temperature increases, the performance of the proposed system from the quality of energy conversion standpoint – that is, the exergy efficiency and sustainability index – will be reduced. This is rational given that a higher enthalpy of combustion products leads to a lower methane mass flow rate needed to provide the constant power of the gas cycle. In contrast, Fig. 6 shows that a desirable environmental condition is achieved by increasing the combustion temperature from 1300 K to 1500 K. The figure further demonstrates that the variation of combustion temperature has a relatively neutral effect on the net power produced, which is increased less than 40 kW. What stands out from Fig. 6(d) is that when the combustion temperature increases, the generated potable water decreases from 2.76

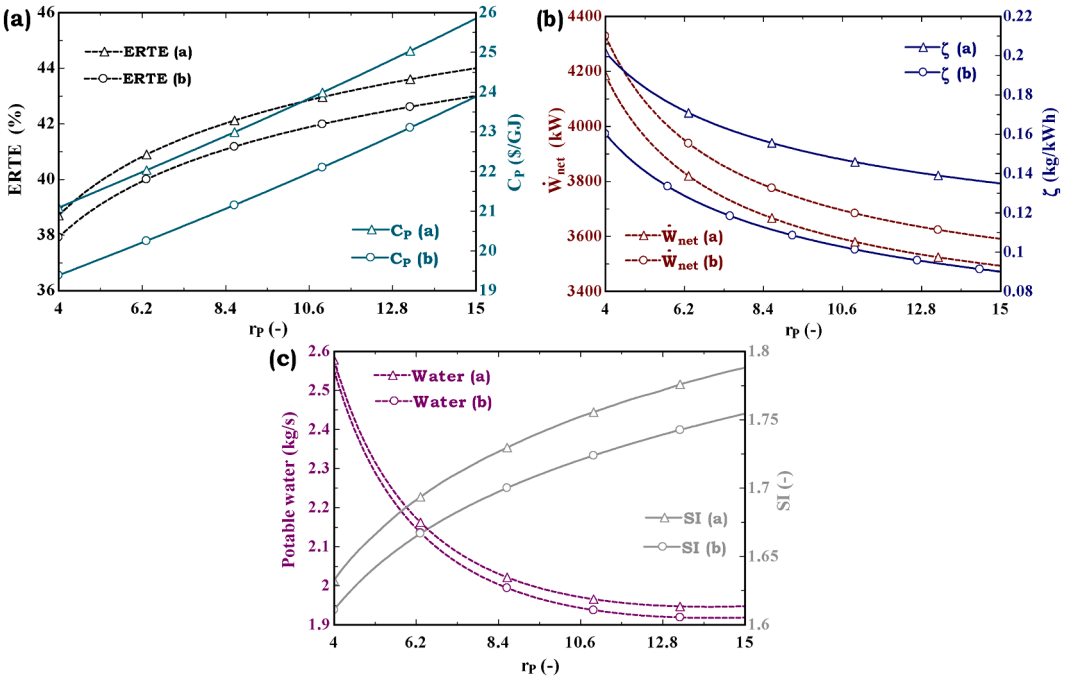

Fig. 5. The variation of techno-economic-environmental indicators with the gas cycle pressure ratio.

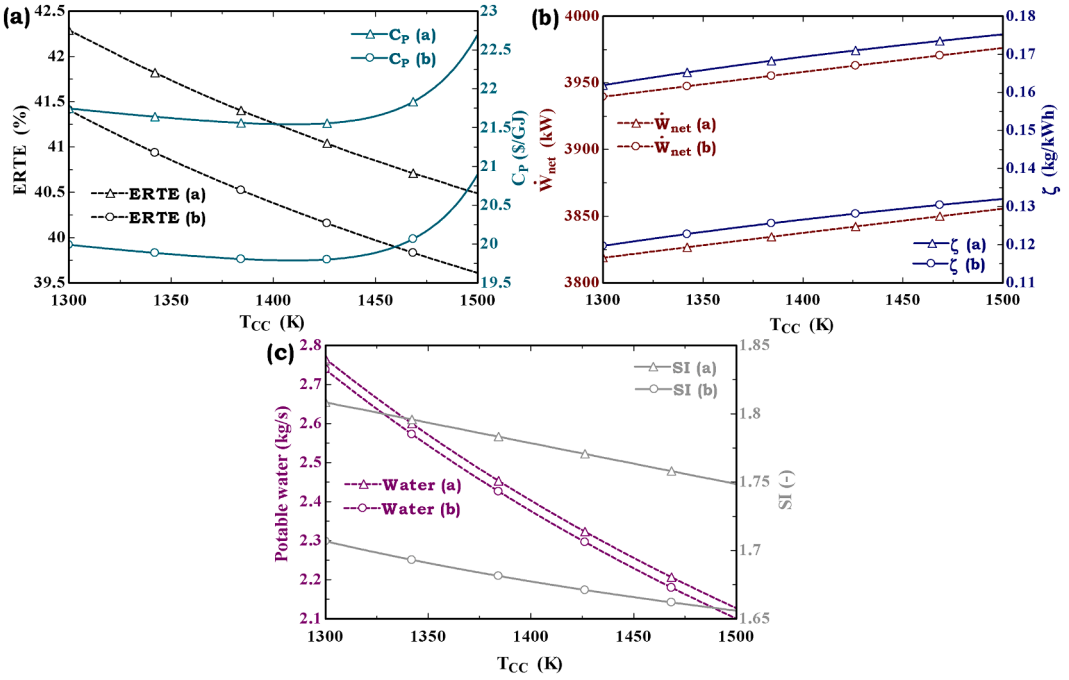

Fig. 6. The variation of techno-economic-environmental indicators with the combustion temperature.

kg/s and 2.73 kg/s to 2.12 kg/s and 2.10 kg/s for the conventional (Model (a)) and proposed innovative (Model (b)) systems, respectively. Eventually, Fig. 6(a) reveals that by increasing the temperature from 1300 K to 1415 K, the initial product energy costs of 21.05 $/GJ and 19.95 $/GJ decrease to a particular value and then increase to 21.96 $/GJ and 20.93 $/GJ for Model (a) and Model (b), respectively, which is improper.

Fig. 7 refers to the effect of the receiver temperature, which is a significant parameter influencing the solar collector performance. A higher receiver temperature results in a higher heat loss from the solar system (see Eq. (4)); hence, the net heat received by the working fluid as well as the mass flow rate entering the receiver will decrease, as inferred from Eq. (6). When the heat gained by the receiver reduces, the rate of input exergy ($\dot{E}_{Sun}$) also decreases. Therefore, as presented in Fig. 7(a), the exergy round trip efficiency will increase. The figure further shows that the rise in the receiver temperature is economically unfavorable because of the solar system's purchased cost growth, which is a function of the operating temperature. According to Fig. 7(b), as the receiver temperature increases from 1200 K to 1250 K, the net power produced rises slightly and subsequently decreases dramatically. This is reasonable because a lower heat is transferred to the Rankine Cycle 1 due to the mass flow rate reduction of the solar system's working fluid entering the

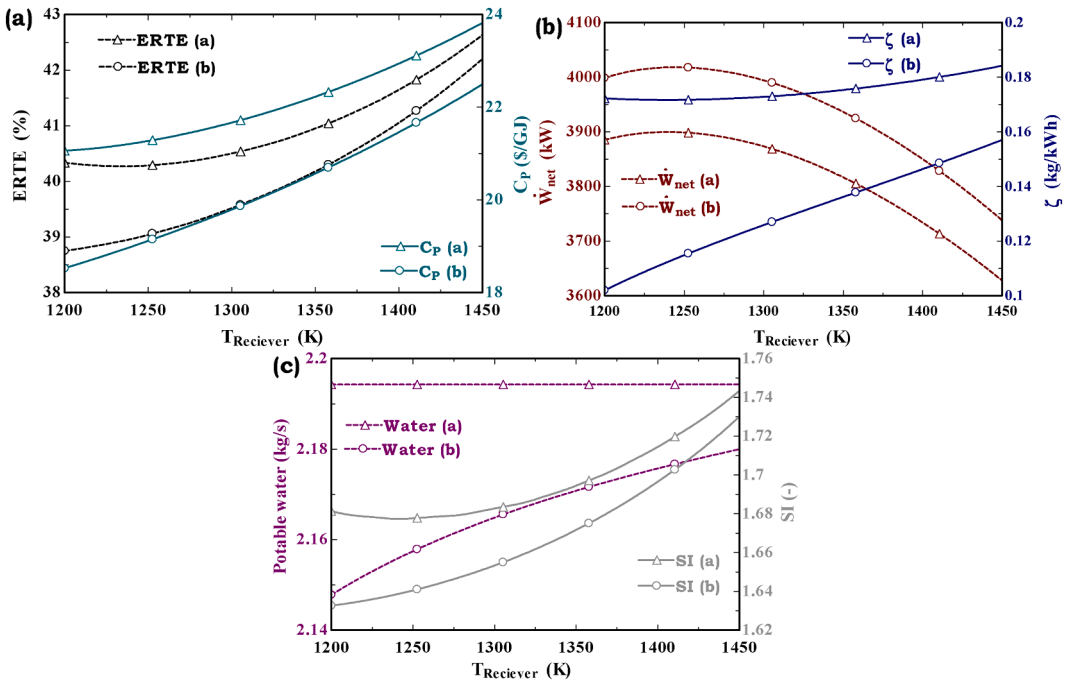

Fig. 7. The variation of techno-economic-environmental indicators with the receiver temperature.

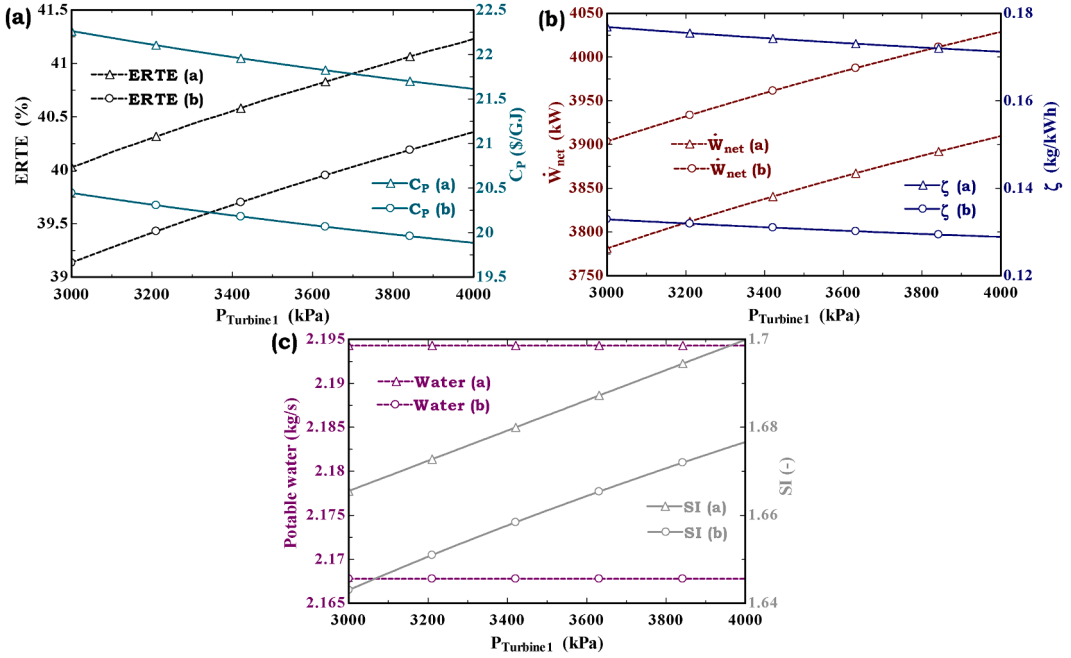

Fig. 8. The variation of techno-economic-environmental indicators with the turbine inlet pressure.

evaporator.

Moreover, by increasing the receiver temperature – that is, the reduction of mass flow rate – lower hydrogen is generated by the VCl cycle. So, higher methane is needed to supply the gas cycle. Accordingly, the increase of receiver temperature is undesirable from the environmental point of view due to more CO_2 being emitted into the atmosphere, as depicted in the figure. According to Fig. 7(c), while the increase in the receiver temperature leads to a higher potable water generation in Model (b), the performance of the MED unit in Model (a) is independent of the solar system design parameters. Finally, the figure demonstrates that a higher sustainability index is achieved for both models by increasing the receiver temperature from 1200 K to 1450 K.

Greater turbine inlet pressure leads to a higher steam enthalpy; therefore, the exergy round trip efficiency and the net power produced will increase, as shown in Fig. 8(a) and(b). Fig. 8 also reveals that the increase in turbine inlet pressure positively affects the product energy cost despite the increase in turbine purchased cost, which is a function of turbine capacity. This is justified because the increase in total exergy produced is more than the total cost rate growth. According to the right-hand side of Fig. 8(b), the increase in inlet pressure is environmentally suitable since the levelized carbon dioxide emission of the conventional and proposed systems falls about 5.2 kg/MWh and 4 kg/MWh,

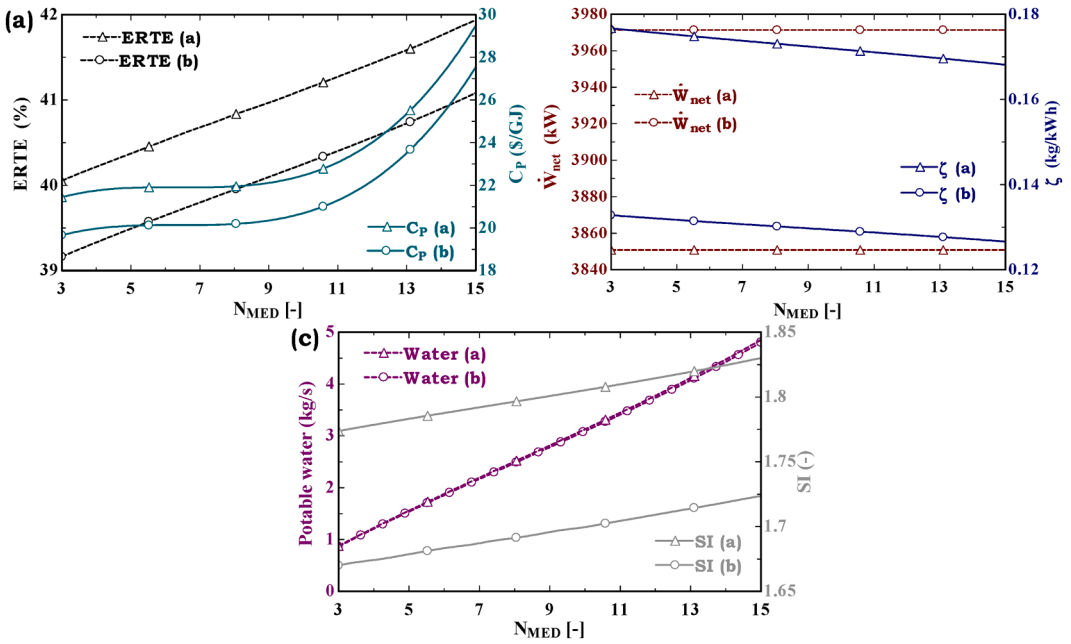

Fig. 9. The variation of techno-economic-environmental indicators with the number of MED effects.

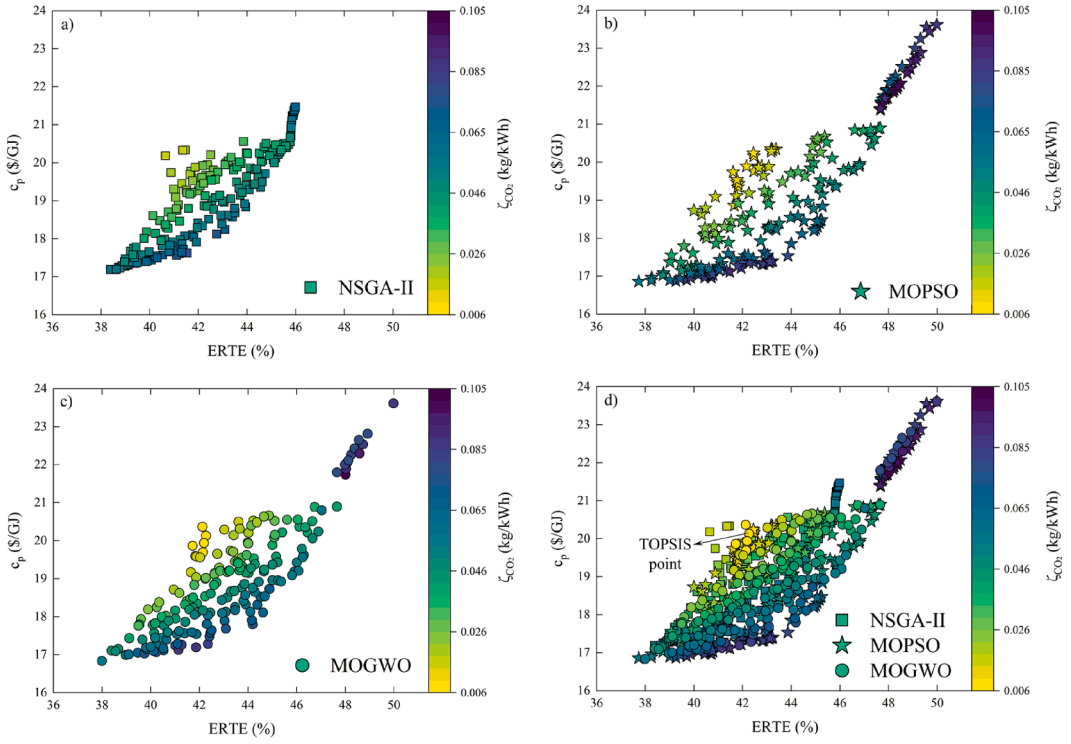

Fig. 10. Three-dimensional Pareto frontier diagram of ETRE, product unit cost, and levelized CO_2 emission based on NSGA-II, MOPSO, and MOGWO approaches.

respectively. Fig. 8(c) depicts that each system's sustainability index increases as the turbine inlet pressure increases because the rate of total exergy destruction declines for a constant input exergy value. Finally, Fig. 8 shows that the rate of potable water production is independent of the variation of turbine pressure. It can be concluded that, like the previous figures, in all turbine inlet pressure domains, the substitution of hydrogen with methane fuel (Model (b)) leads to a considerable lower product energy cost and levelized carbon dioxide emission compared to the fully methane-fueled system (Model (a)). The figure also shows that, in Model (b), the higher power production of 130 kW is attained, indicating the significance of adding TEG for surplus electricity generation from waste heat.

The influence of the number of MED effects in the performance of each model from thermodynamic, economic, and environmental points of view is demonstrated in Fig. 9. According to the figure, as the number of effects increases from 3 to 15, the rate of potable water produced for both models increases by more than 4 kg/s, which is considerable. The figure also shows that when the number of effects rises, the methane-based and proposed innovative models' exergy efficiency increases from 40.05% and 39.16% to 41.94% and 41.08%, respectively, due to

Table 6
Detailed information of TOPSIS point.

Optimization parameters					
PR **(-)**	T_{CC} **(K)**	N_{Hel} **(-)**	$T_{Reciever}$ **(K)**	P_{16} **(kPa)**	P_{24} **(kPa)**
11.75	1200	400	1100	3807	4000

Objective functions		
ERTE **(%)**	C_P **($/GJ)**	ζ_{CO2} **(kg/MWh)**
42.27	20.13	6.7

Important results		
$\dot{m}_{Hydrogen}$ **(kg/s)**	$\dot{m}_{Freshwater}$ **(kg/s)**	$\dot{W}_{net}$ **(kW)**
0.0266	3.11	3854

Table 7
The comparison of techno-economic-environmental indicators at TOPSIS point.

System	***ERTE*** **(%)**	***LCoE*** **($/kWh)**	ζ_{CO2} **(kg/MWh)**
Present model	42.27	72.64	6.7
Bet Sarkis and Zare [37]	36.91	79.34	620
Alirahmi et al. [38]	26.7	35.8	400

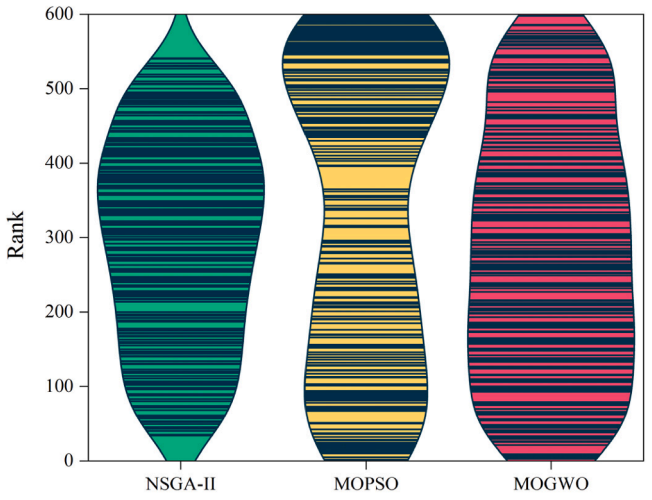

Fig. 11. The ranking of optimum points for each algorithm based on TOPSIS criteria.

the increment in potable water generation rate. According to Fig. 9(a), for both systems, when the number of effects increases from 3 to 9, the product energy costs increase by about 0.5 $/GJ and then rise considerably (more than 7 $/GJ), which is unfavorable. This is defensible because the increment of the total cost rate (the numerator of Eq. (46)), as a function of the number of effects, is higher than the rise of the net exergy produced (denominator of Eq. (46)). Fig. 9 also indicates that the net power produced remains constant by varying the number of effects. More MED effects lead to an upper rate of useful exergy; hence, based on Eq. (48), a lower levelized CO_2 emission is achieved, as illustrated in Fig. 9(b). The simultaneous increase in the product energy cost, which is unfavorable, and the exergy round trip efficiency, which is favorable, clarifies the worth of multi-criteria optimization trying to satisfy both conflictive objectives.

After performing a complete comparative techno-economic-environmental assessment, the proposed system equipped with a TEG unit and an innovative method of greenhouse gas emission reduction is shown to be the superior option compared to the conventional model, due to the higher power produced and considerable lower levelized CO_2 emission and lower product energy cost. Below, three optimization algorithms are applied to the proposed system to find the best operating condition. Then, the feasibility of the proposed system under the optimum design parameters extracted by the best algorithm is examined for Sevilla.

4.3. Optimization results

Multi-objective optimization based on different algorithms is applied to the proposed system to investigate two significant aims: to compare the performance of each optimization algorithm and find the best competent one and reach the most favorable operating condition. For this, Fig. 10 illustrates the Pareto frontier diagram of ERTE, product unit cost, and levelized CO_2 emission applying NSGA-II, MOPSO, and MOGWO algorithms. As shown, the results of the three optimization algorithms are somewhat analogous to each other. However, the optimum points extracted by the NSGA-II (see Fig. 10(a)) are distributed in a more limited domain than the other methods. According to Fig. 10, each curve comprises many optimum points prioritized based on the policy of decision-makers. Because the ideal point, having the maximum ERTE and minimum product unit cost and minimum levelized CO_2 emission simultaneously, is not on the curve, decision criteria must be implemented to find the best optimization point. Among the different tools, TOPSIS, as a multiple attribute decision-making technique, would be a promising option that ranks the optimum points based on their distance from the ideal solution (shortest distance) and negative-ideal solution (farthest distance). Fig. 10(d) depicts the Pareto frontier diagrams of NSGA-II, MOPSO, and MOGWO to compare the optimization results better. According to the figure, the best TOPSIS point with the highest ERTE and lowest product cost and CO_2 emission simultaneously alludes to the MOGWO algorithm.

Table 6 indicates the detailed Pareto frontier information, containing the optimum values of objectives and main operational parameters at the TOPSIS point. According to the table, the optimum values of ERTE, product energy cost, and levelized CO_2 emission are 42.27%, 20.13 $/GJ, and 0.0067 kg/kWh, respectively.

Table 7 compares ETRE, product unit cost, and levelized CO_2 emission obtained by the present system at TOPSIS point against two similar works in the literature. According to Table 7, the proposed multi-generation system is superior to the reference [37] due to lower 613.3 kg/MWh CO_2 emission and 6.7 $/kWh levelized cost of electricity and simultaneously higher exergy efficiency of 5.36%. Table 7 further indicates that despite a higher electricity cost, the present model is superior to the system studied in the reference [38] because of lower CO_2 emission and higher exergy efficiency of 393.3 kg/MWh and 15.57%, which are considerable. However, there are a couple of limitations in such systems that prevent exergy efficiency increment while reducing the cost and CO_2 emission to the desired values obtained by optimization. The first limit is solar availability and the high rate of heat loss – the low energy conversion rate – in the solar system. Next is the domain of decision parameters that cannot be increased/decreased up to a certain value. For instance, the increment of combustion chamber temperature is restricted due to material limitations, or at high turbine inlet pressure values, the superheat fluid cannot be produced.

The contribution of each algorithm from the optimum points based on the TOPSIS criteria is demonstrated in Fig. 11 to more effectively compare the performance of optimization methods. According to the figure, MOGWO presents the best performance because it has a broader surface for lower-ranking points. The thin surface of NSGA-II reveals that it does not work well compared to MOPSO and MOGWO approaches despite wide-ranging applications in optimizing energy systems.

The last but not least significant optimization result is the scatter distribution of main operational parameters to illustrate the distribution of optimum points across the population size, as shown in Fig. 12. According to Fig. 12(a) and 12(c), the compressor pressure ratio and the number of heliostat fields are insensitive parameters because their

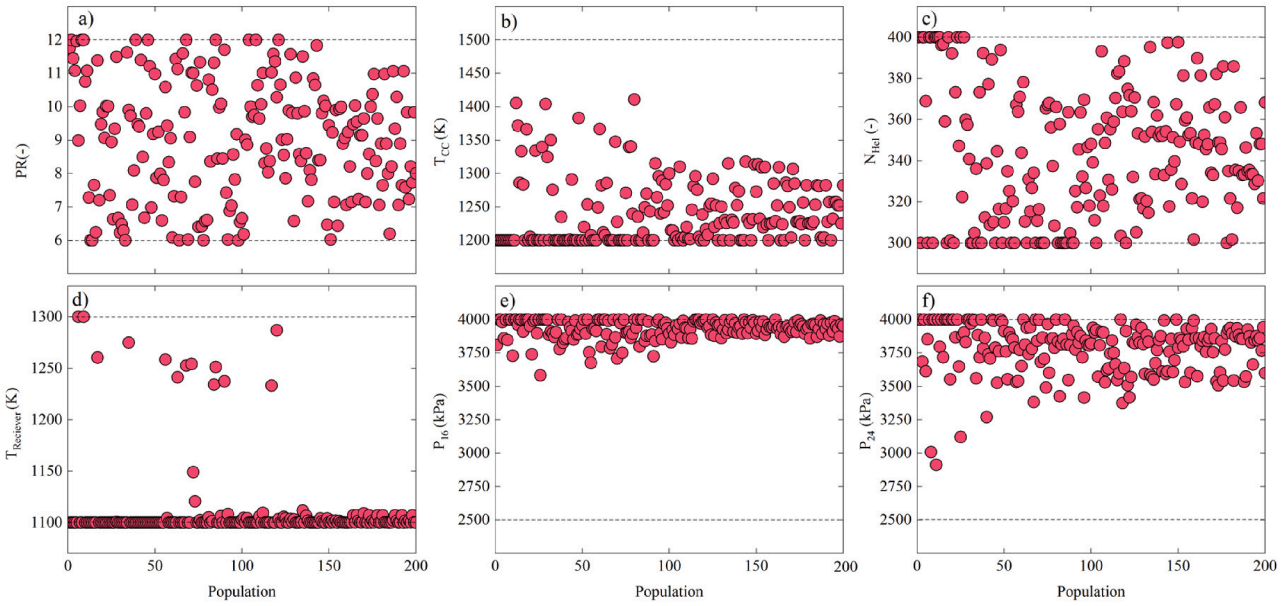

Fig. 12. The scatter distribution of main operating parameters, including a) compressor pressure ratio, b) combustion temperature, c) the number of the heliostat field, d) receiver temperature, e) Turbine 1 inlet pressure, and f) Turbine 2 inlet pressure.

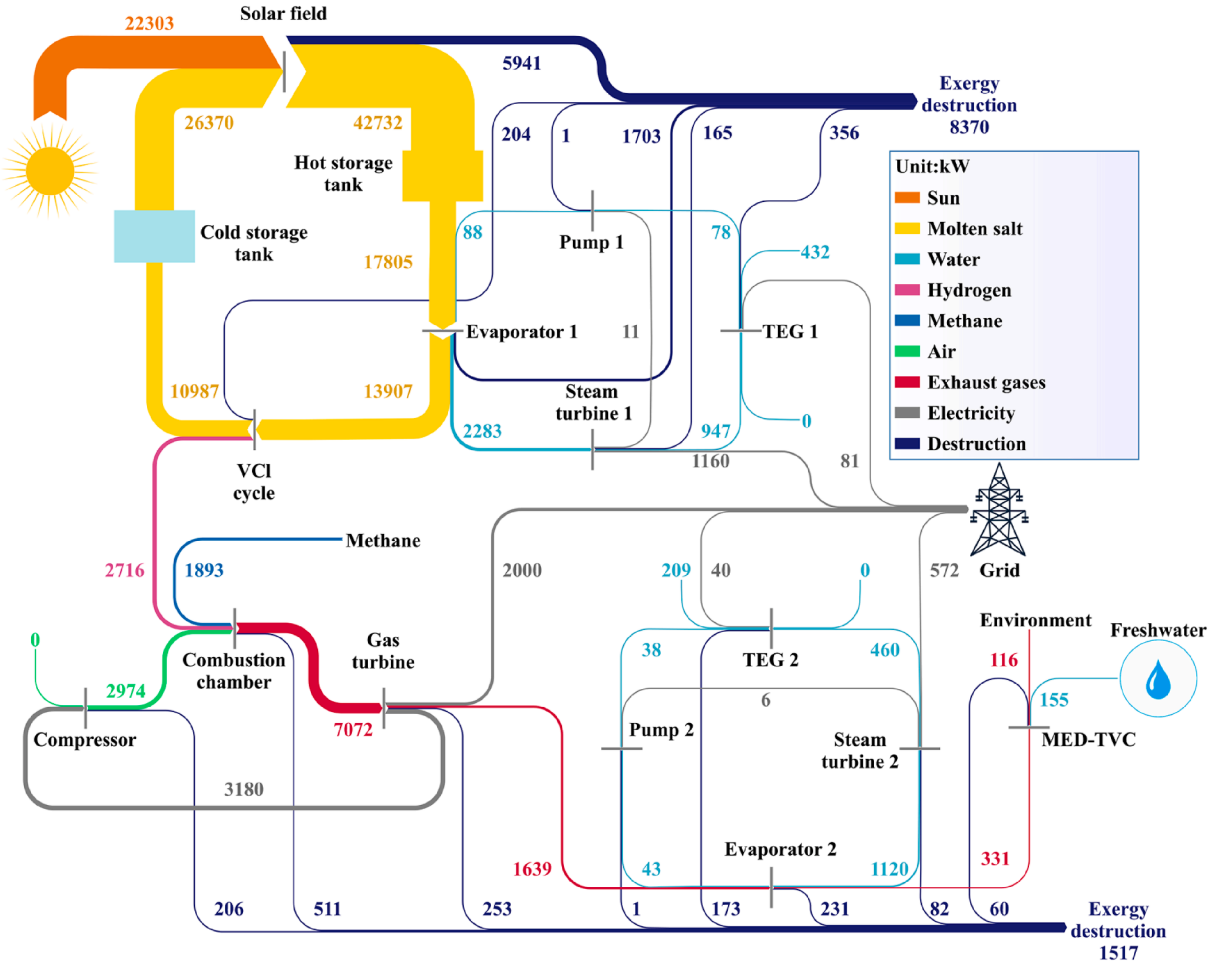

Fig. 13. Sankey diagram illustrating the exergy flow through the proposed innovative system.

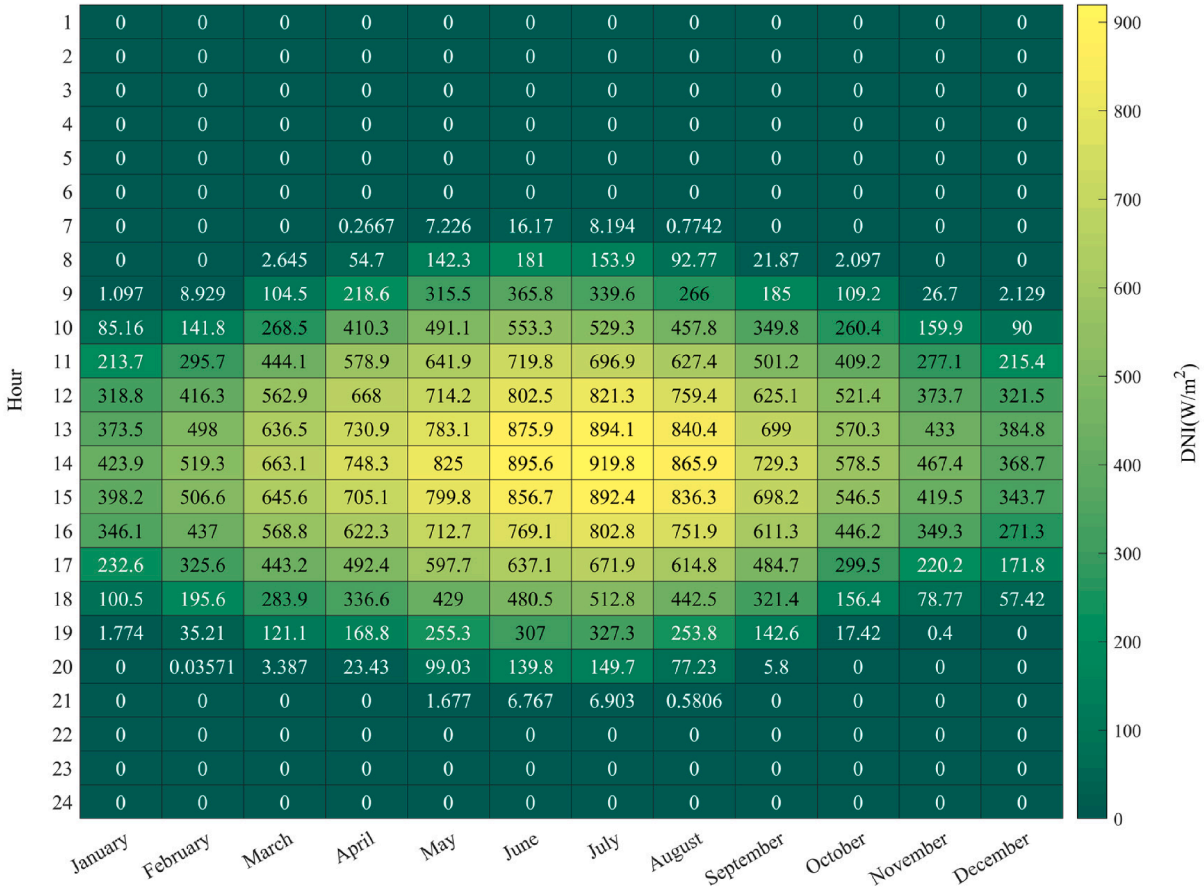

Hour	January	February	March	April	May	June	July	August	September	October	November	December
1	0	0	0	0	0	0	0	0	0	0	0	0
2	0	0	0	0	0	0	0	0	0	0	0	0
3	0	0	0	0	0	0	0	0	0	0	0	0
4	0	0	0	0	0	0	0	0	0	0	0	0
5	0	0	0	0	0	0	0	0	0	0	0	0
6	0	0	0	0	0	0	0	0	0	0	0	0
7	0	0	0	0.2667	7.226	16.17	8.194	0.7742	0	0	0	0
8	0	0	2.645	54.7	142.3	181	153.9	92.77	21.87	2.097	0	0
9	1.097	8.929	104.5	218.6	315.5	365.8	339.6	266	185	109.2	26.7	2.129
10	85.16	141.8	268.5	410.3	491.1	553.3	529.3	457.8	349.8	260.4	159.9	90
11	213.7	295.7	444.1	578.9	641.9	719.8	696.9	627.4	501.2	409.2	277.1	215.4
12	318.8	416.3	562.9	668	714.2	802.5	821.3	759.4	625.1	521.4	373.7	321.5
13	373.5	498	636.5	730.9	783.1	875.9	894.1	840.4	699	570.3	433	384.8
14	423.9	519.3	663.1	748.3	825	895.6	919.8	865.9	729.3	578.5	467.4	368.7
15	398.2	506.6	645.6	705.1	799.8	856.7	892.4	836.3	698.2	546.5	419.5	343.7
16	346.1	437	568.8	622.3	712.7	769.1	802.8	751.9	611.3	446.2	349.3	271.3
17	232.6	325.6	443.2	492.4	597.7	637.1	671.9	614.8	484.7	299.5	220.2	171.8
18	100.5	195.6	283.9	336.6	429	480.5	512.8	442.5	321.4	156.4	78.77	57.42
19	1.774	35.21	121.1	168.8	255.3	307	327.3	253.8	142.6	17.42	0.4	0
20	0	0.03571	3.387	23.43	99.03	139.8	149.7	77.23	5.8	0	0	0
21	0	0	0	0	1.677	6.767	6.903	0.5806	0	0	0	0
22	0	0	0	0	0	0	0	0	0	0	0	0
23	0	0	0	0	0	0	0	0	0	0	0	0
24	0	0	0	0	0	0	0	0	0	0	0	0

Fig. 14. Hourly and monthly variation of direct normal irradiance for Sevilla.

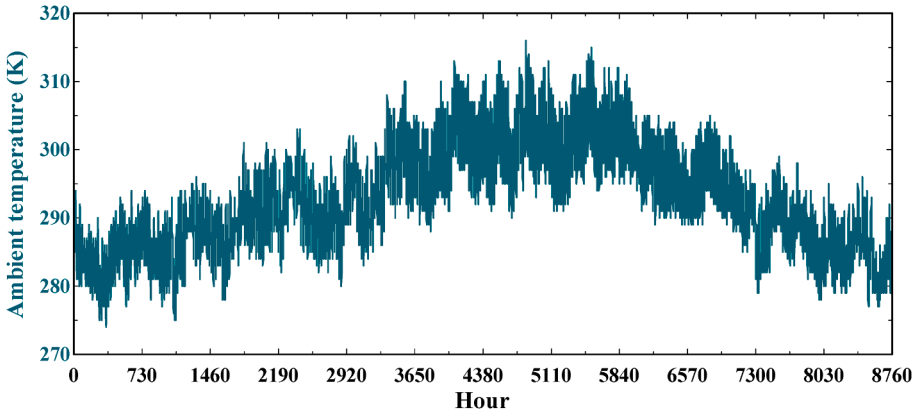

Fig. 15. Hourly variation of ambient temperature for Sevilla.

optimum points are scattered in the entire domain. Moreover, Fig. 12(b) shows that the combustion temperature should be kept at less than 1300 K in order to reach the best techno-economic-environmental condition. Fig. 12(d) and Fig. 12(e) indicate that since the majority of optimum points are adjacent to the lowest and highest domains, the receiver temperature and Steam Turbine 1 inlet pressure are effective parameters, and their variation will change the system's performance. Finally, Fig. 12(f) demonstrates that the optimum points of Steam Turbine 2 inlet pressure are dispersed between 3000 kPa and 4000 kPa, while most are close to the upper bound.

After conducting a throughout optimization, the detailed results of exergy evaluation in the form of the Sankey diagram are demonstrated at the TOPSIS point, as shown in Fig. 13. According to the second law of thermodynamics, chemical reaction, mixing, and higher temperature differences between the hot/cold streams lead to a higher exergy destruction rate (irreversibility). The figure indicates that the solar system with an exergy destruction rate of 5941 kW (around 60% of destructions) is the main component of irreversibility due to the high-temperature difference between the sun and working fluid. After that, the highest destruction rate corresponds to evaporator 1 with 1703 kW. The figure further reveals that the combustion chamber is another deficient device from the quality of energy conversion facet, with the third-highest destruction rate of 231 kW. This is rational due to the mixing inlet fluids and the high-temperature difference between the combustion products and reactants. According to the figure, the high exergy value of the gas turbine outlet stream (1639 kW) shows that the

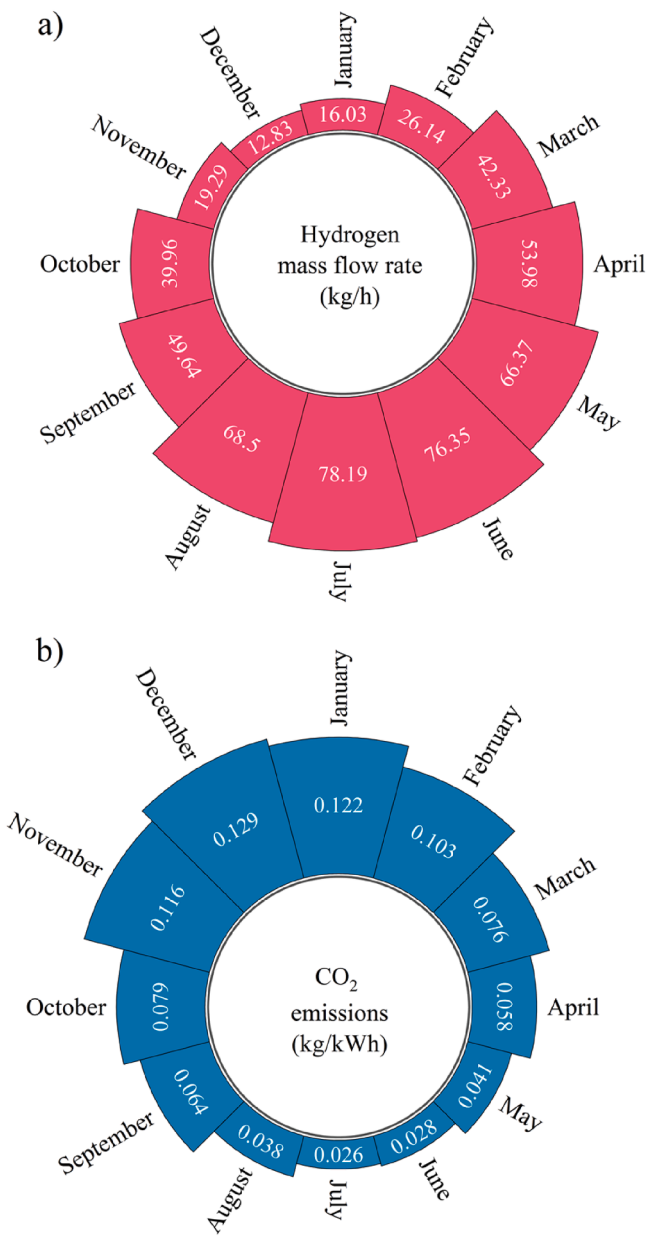

Fig. 16. Calculated values of monthly (a) produced hydrogen mass flow rate and (b) levelized CO_2 emissions for Sevilla, Spain.

flue gas condensation process, as a passive performance enhancement approach, is of great significance for exploiting the waste energy for other uses. It can also be observed that the pump with zero exergy destruction is the highest quality component from the irreversibility point of view since there is no chemical reaction and mixing of the fluids. In this component, the only source of irreversibility is the negligible temperature difference between outlet and inlet fluids. Finally, the figure reveals that by adding Rankine Cycle 2 and the MED unit in the bottom cycle, the value of exergy loss decreases more than 53.2%, which is considerable.

5. Case study

After detecting the superiority of the proposed innovative system, its practicability was examined considering the case of Sevilla, Spain, based on the real ambient data and optimum values attained in the previous section. The hourly and monthly variation of direct normal irradiance (DNI), as a required input data to fulfill the simulation, is depicted in Fig. 14. According to the figure, the highest solar radiation can be obtained in July, where the maximum DNI reaches up to 919.8 W/m^2 at 2p.m. However, the minimum radiation corresponds to December due to the lowest solar availability. Moreover, the hourly variation of ambient temperature, which is another prerequisite data, is demonstrated in Fig. 15. Based on the figure, the local temperature increases from winter to summer and then falls. In this regard, while the maximum ambient temperature is 316.31 K at the 4841st hour of the year, the minimum temperature of 274.43 is obtained at the 345th hour.

Fig. 16 illustrates the monthly variation of the produced hydrogen mass rate, along with the levelized carbon dioxide emitted to the atmosphere, to better indicate the influence of ambient conditions on the performance of the proposed system. By increasing the solar radiation from winter to summer, higher heat is received by the collector's working fluid. Thus, the rate of energy transferred to the VCl cycle and then the hydrogen production rate will increase, as shown in Fig. 16. According to the figure, the highest and lowest monthly hydrogen productions are 78.19 kg/h and 12.83 kg/h in July and December. Higher solar availability leads to a lower natural gas required to provide the gas turbine power demand; therefore, the monthly CO_2 emission reduces from winter to summer. What stands out from the figure is that the minimum CO_2 emission of 0.026 kg/kWh and 0.028 kg/kWh is obtained in July and June, respectively. In contrast, the levelized emission rises to 0.129 kg/kWh and 0.122 kg/kWh in December and January. Comparing monthly levelized CO_2 emitted by the present model against the similar work in the literature [39] indicates that the present study is a promising system from an environmental standpoint. According to the results obtained by Farrokhi et al. [39], the lowest and highest monthly emissions are 0.085 kg/kWh and 0.17 kg/kWh, respectively, which are 0.059 kg/kWh and 0.041 kg/kWh higher than the corresponding values of the present model.

6. Conclusion

The present study introduced an innovative green and cost-effective multi-generation system consisting of the CRCS, VCl thermochemical cycle, TEG, and the MED unit to obtain a lower emission and higher power production. The performance of the suggested system was studied and compared against the configuration driven by the natural gas and equipped with a condenser from thermodynamic, exergoeconomic, sustainability, and environmental points of view. The comparison was conducted through a parametric study that evaluated the effect of the main operational variables on power produced, ERTE, product energy cost, sustainability index, and levelized CO_2 emission. Next, multi-objective optimization based on three algorithms – NSGA-II, MOPSO, and MOGWO – was implemented to the superior model to determine the most competent method and attain the best operating condition according to the TOPSIS criteria. Finally, the performance of the superior model under the optimum decision parameters was investigated considering the case of Sevilla. The significant findings of the techno-economic-environmental parametric comparison are as follows:

- The suggested model equipped with a novel greenhouse gas emission reduction technique is superior to the methane-driven system in terms of economic and environmental aspects due to the lower product unit cost and lower levelized carbon dioxide emission.
- Higher power production reveals that, in addition to the cost-effectiveness and environmental friendliness, integrating the proposed novel configuration with the thermoelectric generator is a promising option from a performance standpoint.
- A higher compressor pressure ratio and lower combustion temperature lead to a considerably higher sustainability index. However, unfavorable economic conditions are achieved due to the increased product energy cost.

The main optimization results are summarized as follows:

- Based on the TOPSIS, the MOGWO algorithm is the most competent multi-objective optimization approach with the highest ERTE and lowest product cost and CO_2 emission simultaneously. Despite widespread application, the worst option is NSGA-II because of the lowest share in high-ranking points.
- Multi-objective optimization of the proposed model based on the grey wolf algorithm results in 2.5% higher ERTE, 1 $/GJ lower product energy cost, and 0.12 kg/kWh lower levelized CO_2 emission compared to the operating condition.
- According to the scatter distribution of main operational parameters, pressure ratio and the number of heliostats are not sensitive parameters. However, the receiver temperature and steam turbine inlet pressure should be kept at their lowest and highest ranges, respectively.
- From the Sankey diagram, it can be observed that the CRCS system is the worst component from an irreversibility viewpoint because of the highest exergy destruction rate of 5941 kW, which is equal to 60% of destructions.

The main findings of transient analysis could be outlined as follows:

- The proposed innovative system is a feasible green solution, especially in warmer climates, to make a large jump toward decarbonization and higher penetration of renewable energy in the global energy matrix.
- By rising the solar radiation from cold to hot months, the rate of hydrogen produced increases dramatically (more than 500 % increment). Also, the levelized CO_2 emission reduces from 0.129 kg/kWh to 0.026 kg/kWh due to lower methane consumption.

Finally, some recommendations for future extensions of the current study are as follows:

- To carry out the advanced exergy or exergo-environmental assessments to compare each model's from the quality of energy conversion in further detail.
- To introduce/develop a novel/modified algorithm, like the dragonfly, to improve optimization performance and overcome the shortcomings of existing approaches.
- To apply four-objective optimization to the proposed system to find the best operational condition considering more than three conflictive objectives simultaneously.
- To compare the proposed system's performance with other possible renewable-driven scenarios, for instance, a wind turbine integrated with a proton exchange membrane unit for electricity and hydrogen production.

CRediT authorship contribution statement

Amirmohammad Behzadi: Visualization, Methodology, Software, Writing – original draft. **Ehsan Gholamian:** Methodology, Data curation, Validation. **Seyed Mojtaba Alirahmi:** Visualization, Methodology, Software. **Behrouz Nourozi:** Writing – review & editing, Data curation. **Sasan Sadrizadeh:** Writing – review & editing, Supervision.

Declaration of Competing Interest

The authors declare that they have no known competing financial interests or personal relationships that could have appeared to influence the work reported in this paper.

Acknowledgment

The authors are grateful to the Swedish Energy Agency (Energimyndigheten) for partly financing this research study.

Appendix A

The equipment's purchased cost is tabulated in Table A1 to accomplish the economic assessment.

Table A1
The purchased cost correlation for each component [6,18,28].

Component	Purchased cost ($)
Air compressor	$Z_{AC} = \left(\frac{75\dot{m}_1}{0.9-\eta_{is,AC}}\right)\left(\frac{P_2}{P_1}\right)\ln\left(\frac{P_2}{P_1}\right)$
Gas turbine	$Z_{GT} = \left(\frac{479.3\dot{m}_3}{0.92-\eta_{is,GT}}\right)\ln\left(\frac{P_3}{P_4}\right)(1+\exp(0.036T_3-54.4))$
Combustion chamber	$Z_{CC} = 48.64\dot{m}_2(1+exp(0.018T_3-26.4))\frac{1}{0.995-\frac{P_3}{P_2}}$
TEG	$Z_{TEG} = 1500\dot{W}_{TEG}$
Condenser	$Z_{Cond} = 1773\dot{m}_{water}$
Steam turbine	$Z_{ST} = 6000\dot{W}_{ST}^{0.7}$
Pump	$Z_{Pm} = 3540\dot{W}_{Pm}^{0.71}$
Evaporator	$Z_E = 276\left(\frac{\dot{Q}_E}{4.39\Delta T_{ln}}\right)^{0.8}$
Heat exchanger	$Z_{HEX} = 12000\left(\frac{A_{HEX}}{100}\right)^{0.6}$
Solar receiver	$Z_r = A_r(79T_r-42000)$
Solar heliostat	$Z_H = 150A_{Hel}N_{Hel}$
VCl cycle	$Z_{VCl} = 0.125\dot{m}_{21}LHV_{H_2}$
MED ejector	$16.14\times 989\times(\dot{m}_s\left(\frac{T_i}{P_i}\right)^{0.05}P_e^{-0.75})$
MED effects	$201.67\times\dot{Q}(LMTD^{-1}dp_t^{0.15}dp_s^{-0.15})$
MED condenser	$430\times 0.582\times\dot{Q}(LMTD^{-1}dp_t^{0.01}dp_s^{-0.1})$

Appendix B

The standard chemical exergy of gas components used in the present study are listed in Table B1.

Table B1
Standard chemical exergy of gaseous components [40].

Component	e_0^{ch} (kJ/mol)
O_2	3.97
N_2	0.72
H_2	236.09
CH_4	831.2
H_2O	9.5
Cl_2	123.6
HCl	84.5
CO_2	19.48

References

[1] Barbera E, Mio A, Massi Pavan A, Bertucco A, Fermeglia M. Fuelling power plants by natural gas: An analysis of energy efficiency, economical aspects and environmental footprint based on detailed process simulation of the whole carbon capture and storage system. Energy Convers Manag 2022;252:115072. https://doi.org/10.1016/j.enconman.2021.115072.
[2] Liu W, Chen C, Wu H, Guo C, Chen Y, Liu W, et al. Environmental life cycle assessment and techno-economic analysis of domestic hot water systems in China. Energy Convers Manag 2019;199:111943. https://doi.org/10.1016/j.enconman.2019.111943.
[3] Kazancoglu Y, Ozbiltekin-Pala M, Ozkan-Ozen YD. Prediction and evaluation of greenhouse gas emissions for sustainable road transport within Europe. Sustain Cities Soc 2021;70:102924. https://doi.org/10.1016/j.scs.2021.102924.
[4] Al-Othman A, Tawalbeh M, Martis R, Dhou S, Orhan M, Qasim M, et al. Artificial intelligence and numerical models in hybrid renewable energy systems with fuel cells: advances and prospects. Energy Convers Manag 2022;253:115154. https://doi.org/10.1016/j.enconman.2021.115154.

[5] Liang Y, Chen J, Yang Z, Chen J, Luo X, Chen Y. Economic-environmental evaluation and multi-objective optimization of supercritical CO2 based-central tower concentrated solar power system with thermal storage. Energy Convers Manag 2021;238:114140. https://doi.org/10.1016/j.enconman.2021.114140.

[6] Alirahmi SM, Razmi AR, Arabkoohsar A. Comprehensive assessment and multi-objective optimization of a green concept based on a combination of hydrogen and compressed air energy storage (CAES) systems. Renew Sustain Energy Rev 2021; 142:110850. https://doi.org/10.1016/j.rser.2021.110850.

[7] Praveen RP. Performance analysis and optimization of central receiver solar thermal power plants for utility scale power generation. Sustain 2020;12(1):127.

[8] Saghafifar M, Mohammadi K, Powell K. Design and analysis of a dual-receiver direct steam generator solar power tower plant with a flexible heliostat field. Sustain Energy Technol Assessm 2020;39:100698. https://doi.org/10.1016/j.seta.2020.100698.

[9] Pashchenko D. Natural gas reforming in thermochemical waste-heat recuperation systems: a review. Energy 2022;251:123854. https://doi.org/10.1016/j.energy.2022.123854.

[10] Pashchenko D. Hydrogen-rich fuel combustion in a swirling flame: CFD-modeling with experimental verification. Int J Hydrogen Energy 2020;45:19996–20003. https://doi.org/10.1016/j.ijhydene.2020.05.113.

[11] Oruc O, Dincer I. Analysis and assessment of a new solar assisted sodium hydroxide thermochemical hydrogen production cycle. Energy Convers Manag 2021;237: 114139. https://doi.org/10.1016/j.enconman.2021.114139.

[12] Sadeghi S, Ghandehariun S, Naterer GF. Exergoeconomic and multi-objective optimization of a solar thermochemical hydrogen production plant with heat recovery. Energy Convers Manag 2020;225:113441. https://doi.org/10.1016/j.enconman.2020.113441.

[13] Balta MT, Dincer I, Hepbasli A. Comparative assessment of various chlorine family thermochemical cycles for hydrogen production. Int J Hydrogen Energy 2016;41: 7802–13. https://doi.org/10.1016/j.ijhydene.2015.12.222.

[14] Behzadi A, Arabkoohsar A, Gholamian E. Multi-criteria optimization of a biomass-fired proton exchange membrane fuel cell integrated with organic rankine cycle/thermoelectric generator using different gasification agents. Energy 2020;201: 117640. https://doi.org/10.1016/j.energy.2020.117640.

[15] Habibollahzade A, Gholamian E, Ahmadi P, Behzadi A. Multi-criteria optimization of an integrated energy system with thermoelectric generator, parabolic trough solar collector and electrolysis for hydrogen production. Int J Hydrogen Energy 2018;43:14140–57. https://doi.org/10.1016/j.ijhydene.2018.05.143.

[16] Demir ME, Dincer I. Development of a hybrid solar thermal system with TEG and PEM electrolyzer for hydrogen and power production. Int J Hydrogen Energy 2017; 42:30044–56. https://doi.org/10.1016/j.ijhydene.2017.09.001.

[17] Khanmohammadi S, Abdi Chaghakaboodi H, Musharavati F. Solar-based Kalina cycle integrated with PEM fuel cell boosted by thermoelectric generator: development and thermodynamic analysis. Int J Green Energy 2021;18:866–78. https://doi.org/10.1080/15435075.2021.1881900.

[18] Behzadi A, Habibollahzade A, Ahmadi P, Gholamian E, Houshfar E. Multi-objective design optimization of a solar based system for electricity, cooling, and hydrogen production. Energy 2019;169:696–709. https://doi.org/10.1016/j.energy.2018.12.047.

[19] Fakhari I, Behzadi A, Gholamian E, Ahmadi P, Arabkoohsar A. Design and tri-objective optimization of a hybrid efficient energy system for tri-generation, based on PEM fuel cell and MED using syngas as a fuel. J Clean Prod 2021;290:125205. https://doi.org/10.1016/j.jclepro.2020.125205.

[20] Youssef PG, Al-Dadah RK, Mahmoud SM. Comparative analysis of desalination technologies. Energy Procedia 2014;61:2604–7. https://doi.org/10.1016/j.egypro.2014.12.258.

[21] Chitgar N, Emadi MA. Development and exergoeconomic evaluation of a SOFC-GT driven multi-generation system to supply residential demands: electricity, fresh water and hydrogen. Int J Hydrogen Energy 2021;46:17932–54. https://doi.org/10.1016/j.ijhydene.2021.02.191.

[22] Aguilar-Jiménez JA, Velázquez N, López-Zavala R, Beltrán R, Hernández-Callejo L, González-Uribe LA, et al. Low-temperature multiple-effect desalination/organic Rankine cycle system with a novel integration for fresh water and electrical energy production. Desalination 2020;477:114269. https://doi.org/10.1016/j.desal.2019.114269.

[23] Orhan MF, Dincer I, Rosen MA. Energy and exergy assessments of the hydrogen production step of a copper–chlorine thermochemical water splitting cycle driven by nuclear-based heat. Int J Hydrogen Energy 2008;33:6456–66. https://doi.org/10.1016/j.ijhydene.2008.08.035.

[24] Arabkoohsar A, Behzadi A, Alsagri AS. Techno-economic analysis and multi-objective optimization of a novel solar-based building energy system; an effort to reach the true meaning of zero-energy buildings. Energy Convers Manag 2021;232: 113858. https://doi.org/10.1016/j.enconman.2021.113858.

[25] Pourrahmani H, Moghimi M. Exergoeconomic analysis and multi-objective optimization of a novel continuous solar-driven hydrogen production system assisted by phase change material thermal storage system. Energy 2019;189: 116170. https://doi.org/10.1016/j.energy.2019.116170.

[26] Balat M. Potential importance of hydrogen as a future solution to environmental and transportation problems. Int J Hydrogen Energy 2008;33:4013–29. https://doi.org/10.1016/j.ijhydene.2008.05.047.

[27] Siddique ARM, Mahmud S, Van HB. A review of the state of the science on wearable thermoelectric power generators (TEGs) and their existing challenges. Renew Sustain Energy Rev 2017;73:730–44. https://doi.org/10.1016/j.rser.2017.01.177.

[28] Jamshidian FJ, Gorjian S, Shafieefar M. Techno-economic assessment of a hybrid RO-MED desalination plant integrated with a solar CHP system. Energy Convers Manag 2022;251:114985. https://doi.org/10.1016/j.enconman.2021.114985.

[29] Wen C, Gong L, Ding H, Yang Y. Steam ejector performance considering phase transition for multi-effect distillation with thermal vapour compression (MED-TVC) desalination system. Appl Energy 2020;279:115831. https://doi.org/10.1016/j.apenergy.2020.115831.

[30] Behzadi A, Arabkoohsar A, Perić VS. Innovative hybrid solar-waste designs for cogeneration of heat and power, an effort for achieving maximum efficiency and renewable integration. Appl Therm Eng 2021;190:116824.

[31] Bahramian F, Akbari A, Nabavi M, Esfandi S, Naeiji E, Issakhov A. Design and tri-objective optimization of an energy plant integrated with near-zero energy building including energy storage: An application of dynamic simulation. Sustain Energy Technol Assessm 2021;47:101419. https://doi.org/10.1016/j.seta.2021.101419.

[32] Sun Z, Wang S, Aziz M. Highly integrated system for ammonia and electricity production from biomass employing direct chemical looping: exergy and exergoeconomic analyses. Energy Convers Manag 2022;251:115013. https://doi.org/10.1016/j.enconman.2021.115013.

[33] Gholamian E, Ahmadi P, Hanafizadeh P, Mazzarella L. The use of waste heat recovery (WHR) options to produce electricity, heating, cooling, and freshwater for residential buildings. Energy Equipment and Systems 2020;8(3):277–96. https://doi.org/10.22059/EES.2020.44949.

[34] Balafkandeh S, Zare V, Gholamian E. Multi-objective optimization of a tri-generation system based on biomass gasification/digestion combined with S-CO2 cycle and absorption chiller. Energy Convers Manag 2019;200:112057. https://doi.org/10.1016/j.enconman.2019.112057.

[35] Ziapour BM, Saadat M, Palideh V, Afzal S. Power generation enhancement in a salinity-gradient solar pond power plant using thermoelectric generator. Energy Convers Manag 2017;136:283–93. https://doi.org/10.1016/j.enconman.2017.01.031.

[36] Moghimi M, Emadi M, Mirzazade Akbarpoor A, Mollaei M. Energy and exergy investigation of a combined cooling, heating, power generation, and seawater desalination system. Appl Therm Eng 2018;140:814–27.

[37] Bet Sarkis R, Zare V. Proposal and analysis of two novel integrated configurations for hybrid solar-biomass power generation systems: thermodynamic and economic evaluation. Energy Convers Manag 2018;160:411–25. https://doi.org/10.1016/j.enconman.2018.01.061.

[38] Alirahmi SM, Khoshnevisan A, Shirazi P, Ahmadi P, Kari D. Soft computing based optimization of a novel solar heliostat integrated energy system using artificial neural networks. Sustain Energy Technol Assessm 2022;50:101850. https://doi.org/10.1016/j.seta.2021.101850.

[39] Farrokhi M, Motallebzadeh R, Javani N, Ebrahimpour A. Dynamic simulation of an integrated energy system for buildings in cold climates with thermal energy storage. Sustain Energy Technol Assessm 2021;47:101459. https://doi.org/10.1016/j.seta.2021.101459.

[40] Al C. Appendix: Standard Chemical Exergy. Thermodyn Destr Resour 2011:489–94. https://doi.org/10.1017/cbo9780511976049.024.

[41] Habibollahzade A, et al. Enhanced performance and reduced payback period of a low grade geothermal-based ORC through employing two TEGs. Energy Equipment and Systems 2019;7(1):23–39. https://doi.org/10.22059/ees.2019.34611.

[42] Gholamian E, et al. Exergo-economic analysis of a hybrid anode and cathode recycling SOFC/Stirling engine for aviation applications. International Journal of Sustainable Aviation 2018;4(1):11–30.

[43] Gholamian E, et al. Analysis and Optimization Proposal of a Typical Building in Tehran Using TRNSYS Software. Easy Chair 2018;(241).